The intracellular domain of the epilepsy-related protein PCDH19 regulates spine density in cortical neurons.

Sylvia A Newbold[1], Ian WJ Fox[1,3], Cristina Llinares-Benadero[1,3], Jaime Fabra-Beser[2], Elizaveta Stebleva[1], Cristina Gil-Sanz[2], Isabel Martinez-Garay[1,2].

[1] Division of Neuroscience, School of Biosciences, Cardiff University, CF10 3AX Cardiff, Wales, United Kingdom

[2] BIOTECMED Institute, Universidad de Valencia, Burjassot, 46100 Valencia, Spain

[3] These authors contributed equally to this work.

Corresponding author: Isabel Martinez-Garay – Isabel.M.Garay@uv.es

Running Title: PCDH19-ICD regulates spine density

ABSTRACT

Mutations in the X-linked cell adhesion molecule Protocadherin 19 (*PCDH19*) lead to epilepsy with cognitive impairment in heterozygous females and post-zygotic mosaic males. A complete absence of functional protein does not elicit symptoms, indicating a complex physiopathology and a dependence on cellular mosaicism. It is believed that mosaic expression of PCDH19 on neuronal membranes leads to defective cell-cell communication in the brain, but whether further roles beyond cell adhesion are critical for PCDH19 function in the cortex is currently unknown. Here, we characterize the proteolytic processing of PCDH19 in mouse cortical-like embryonic stem cell derived neurons and cortical lysates and show that its intracellular domain interacts with importins to be transported into the nucleus. RNAseq analysis of neurons derived from an engineered mouse embryonic stem cell line further indicates that the intracellular domain of PCDH19 leads to broad changes in the transcriptional landscape that are related to neuronal differentiation processes. Finally, we use *in utero* electroporation to provide the first *in vivo* data about the role of this cleaved intracellular domain in upper layer cortical neurons, where it reduces spine density without affecting overall dendritic morphology. Because processing is activity dependent, our results suggest that PCDH19 could act as an activity sensor in a synapse to nucleus signaling pathway involved in synaptic homeostasis.

INTRODUCTION

Cell adhesion molecules (CAMs) play essential roles in the development and functioning of the nervous system. Their ability to mediate homo- or heterophilic binding across the synaptic cleft allows them to connect pre- and postsynaptic neurons and underpins their important function in the formation of new synapses during development. For example, CAMs act as recognition molecules and coordinate synaptic differentiation, both morphologically and molecularly (Dean et al., 2003; Wit and Ghosh, 2016). In the adult brain, CAMs can regulate different aspects of synaptic structure and function, including spine shape, receptor function and synaptic plasticity (Dalva et al., 2007; Thalhammer and Cingolani, 2014). One way in which CAMs accomplish this is through direct interaction with neurotransmitter receptors and scaffolding proteins to modulate receptor surface levels (Nuriya and Huganir, 2006; Saglietti et al., 2007; Fièvre et al., 2016; Bassani et al., 2018). Additionally, the strength of the synapses can be altered by processing through the physical loss of homo- or hetero-interactions across the synaptic cleft (Peixoto et al., 2012; Servián-Morilla et al., 2018) . Finally, proteolytic processing of CAMs can translate neuronal activity into intracellular signalling via activity dependent proteolytic cleavage (Shinoe and Goda, 2015). This phenomenon, in which CAMs are processed by proteases in response to neuronal activity, can activate or suppress CAM-dependent signalling and generate new bioactive fragments with high spatial specificity restricted to active synapses. Numerous CAMs belonging to different families, including cadherins, have been shown to undergo activity dependent proteolytic cleavage (Nagappan-Chettiar et al., 2017). In the cadherin superfamily examples include N-cadherin, PCDHγC3 and Protocadherin 19 (PCDH19) (Marambaud et al., 2003; Reiss et al., 2006; Gerosa et al., 2022). However, the relative contribution of adhesive and nuclear functions to the *in vivo* roles of these CAMs is still unknown. PCDH19 is a member of the cadherin superfamily of cell-cell adhesion proteins (Wolverton and Lalande, 2001). Mutations in this X-linked gene lead to epileptic encephalopathy in heterozygous females and in males with somatic mutations, but do not cause any symptoms in hemizygous males (Juberg and Hellman, 1971; Dibbens et al., 2008; Depienne et al., 2009). This unusual inheritance pattern is believed to be due to a phenomenon called “cellular interference”, in which the coexistence of cells with different genotypes, caused by random X chromosome inactivation in heterozygous females and by the somatic mutation in males, is detrimental at the tissue level, even if mutated cells are not affected themselves (Depienne et al., 2009). PCDH19 can mediate cell adhesion on its own,

but also as a complex with CDH2 (Emond et al., 2011) or other delta protocadherins (Bisogni et al., 2018; Pederick et al., 2018). In addition, PCDH19 has been shown to localize to synapses and to interact with the alpha subunit of the GABA receptor (Hayashi et al., 2017; Bassani et al., 2018), modulating surface availability and affecting postsynaptic inhibitory currents. PCDH19 is also necessary for the formation of mossy fibres (Hoshina et al., 2021).

Beyond its roles at the membrane, PCDH19 has also been reported to interact with the paraspeckle protein NONO and co-regulate ER alpha controlled genes (Pham et al., 2017), and to regulate expression of immediate early genes after proteolytic cleavage (Gerosa et al., 2022). However, the transcriptional pathways regulated by PCDH19 and the *in vivo* consequences of this nuclear function remain unclear. Thus, to better understand the biological significance of PCDH19 non-adhesive functions, we carried out a biochemical characterization of PCDH19 cleavage and a transcriptional analysis of the changes triggered by its intracellular domain (ICD) in cortical neurons. Finally, we conducted *in vivo* functional studies in the mouse neocortex, revealing that PCDH19-ICD regulates spine density in upper layer cortical neurons.

MATERIALS AND METHODS

Animals

C57BL/6J WT mice were purchased from Charles River Laboratories. *Pcdh19* knock-out (KO) mice (TF2108) were purchased from Taconic Biosciences. Animals were housed on a 12 h light/dark cycle and with *ad libitum* access to food and drink. All procedures were conducted in accordance with the Animals (Scientific Procedures) Act1986 (amended 2012). Genotyping was done using the Mouse Direct PCR kit (Biotool, cat no. B4001), following the manufacturer's instructions and using primers *Pcdh19*-WT-F (5'-TAGAGGTTCTTGCTGAAGACTTCC-3'), *Pcdh19*-WT-R (5'-TCAACTGTTTCGATGAGACACTGC-3'), *Pcdh19*-Mut-F (5'-GTGCGTACCAGGCGGGAGC-3') and *Pcdh19*-Mut-R (5'-CCCTAGGAATGCTCGTCAAGA-3').

Plasmids

pcDNA-PCDH19-Gal4DBD-VP16 was created by In-Fusion cloning (Takara Bio) using PCDH19-FL and Gal4DBD-VP16 PCR products and a pcDNA vector digested with BamHI and EcoRI. The

Gal4DBD-VP16 fragment was amplified from Gal4-VP16, a gift from Lea Sistonen (Addgene plasmid # 71728) (Budzyński et al., 2015). pGL2-GAL4-UAS-Luc was a gift from Martin Walsh (Addgene plasmid # 33020) (Nishio and Walsh, 2004) pMet7-IFNAR1-Gal4-VP16 and pMet7-IFNAR2-Gal4-VP16 plasmids (the controls for the cleavage luciferase reporter assay) were kind gifts from the Tavernier lab, Ghent, Belgium and pRL-TK was acquired from Promega.

pPB (encoding the piggyBac transposase) was obtained from the Wellcome Trust Sanger Institute (Prosser et al., 2011). pPB-CAG-MbEGFP and pPB-CAG-EGFP (to allow genomic insertion of membrane or regular EGFP) were kind gifts from Dr Fernando García-Moreno. pX330sgRNA#2 was generated by annealing oligonucleotides sgRNA2-*Pcdh19Cterm*-F (5'-CACCGTATCGTTCTCTAAAGCCATC-3') and sgRNA2-*Pcdh19Cterm*-R (5'-AAACGATGGCTTTAGAGAACGATAc-3') and ligating them into the BbsI site of pX330. pX330-U6-Chimeric_BB-CBh-hSpCas9 (also called pX330 or pSpCas9(BB)) was a gift from Feng Zhang (Addgene plasmid # 42230) (Cong et al., 2013).

pLeakless-III-19-HA (the targeting vector to generate endogenous PCDH19-HA) contains the last 487 bp from *Pcdh19* intron 5, followed by the coding region of exon 6 fused to an HA-tag and 1574 bp from *Pcdh19* 3'UTR inserted into the EcoRV site. pLeakless-III was a kind gift of Dr Fumio Matsuzaki (Tsunekawa et al., 2016).

pCAGIG (pCIG) was a gift from Connie Cepko (Addgene plasmid # 11159) (Matsuda and Cepko, 2004) and pCBA-PCDH19FL-HA contains full length mouse PCDH19 (including exon 2) fused C-terminally with an HA tag under the control of the Chicken β-actin promotor. pCBA-PCDH19ICD-HA is the same plasmid, but contains PCDH19 aa 700 to 1145 with an added methionine at the beginning. To create pCBA-PCDH19ICD(NLSmut)-HA, the last four basic residues of the predicted NLS (aa 777 to 780 of the FL protein) were mutated via PCR from "KKKK" to "AAAA" in the PCDH19-ICD-HA construct. KPNA1-myc was purchased from Origene (CAT#: MR208599).

To create pZDRosa-floxedNeo-Pcdh19-CYTO-HA (the targeting vector for PCDH19-ICD-HA overexpression from the *Rosa26* locus), the pZDRosa-floxedNeo-IRES-EGFP plasmid (kind gift of Dr Xinsheng Nan) was linearized and the IRES-EGFP fragment was excised by double restriction digestion with BsrGI-HF and AscI. The PCDH19ICD-HA fragment was amplified from the pre-existing plasmid pCIG-19ICD-HA using primers Rosa26-CYTO-HA-F2 (5'-ACCTCGAGTGGCGCGCCGCGCAGCCATGGCAATGGCAATCAAATGC

-3') and Rosa26-CYTO-HA-R (5'- CCGCTTTACTTGTACTCAAGCGTAATCTGGAACATCGTATG -3'). The resulting PCR product was cloned between the 3' and 5' arms of the *Rosa26* targeting vector using In-Fusion cloning (Takara Bio). Plasmid sequence was checked by sequencing. pCMV-RosaR4 KKR mutations and pCMV-RosaL6 ELD mutations were gifts from Charles Gersbach (Addgene plasmids # 37199 and # 37198) (Perez-Pinera et al., 2012)

Cell culture, transfection and drug treatment

Cells in culture were routinely tested for mycoplasma infection with Lookout Mycoplasma PCR detection kit (Sigma, MP0035), following the manufacturer's instructions. HEK293 and HeLa cells were maintained in CA media (DMEM + 1% non-essential amino acids + 1% L-Glutamine + 10% FBS heat inactivated + 1.43 mM-β-mercaptoethanol) on 100 mm (Nunc) dishes. For 6 well plates, ~500,000 cells were split into each well. For 12 well and 24 well plates, ~250,000 and ~50,000 cells were split into each well, respectively. Cells were transfected 24 hours after seeding using Lipofectamine™ 2000 (Thermo Fisher) at a 1:2 ratio (DNA: Lipofectamine). 1 µg and 500 ng of DNA were used for each plasmid for co-immunoprecipitation (CoIP) and immunocytochemistry (ICC) experiments, respectively.

Cells (HeLa cells and/or mESC-derived neurons) were subjected to the following treatments: Ionomycin (Sigma, I3909) 5 µM for 10 min, 30 min or 60 min; GI254023X (Sigma, SML0789) 10 µM for 1h; MK-8931 (Stratech, B6195-APE) 10 µM for 1h; BB-94 (Stratech, A2577-APE) 10 µM for 1h; DAPT (Sigma, D5942) 10 µM for 16h, Calpeptin (Sigma, C8999) 20 µM for 16h, NMDA (Sigma, M3262) 50 µM for 30 min and (+)-MK-801 maleate (Tocris, 0924) 1 µM for 30 min.

Cleavage luciferase reporter assay

HEK293 cells (5×10^4 HEK293T cells/well in a 24-well plate) were transfected with 150 ng pGL2-Gal4-UAS-Luc, 5 ng pRL-TK and 150 ng of the appropriate Gal4-VP16 fused constructs: pcDNA-PCDH19-Gal4-VP16, pMet7-IFNAR1-Gal4-VP16 and pMet7-IFNAR2-Gal4-VP16 using Lipofectamine™ 3000. Firefly and Renilla luminescence activities were measured one day after transfection using the Dual Luciferase Reporter Assay System (Promega), following the passive cell lysis protocol. Measurements were performed with a FLUOstar Omega microplate reader (BMG Labtech). Firefly

values were normalized to Renilla values and expressed as relative fluorescence units. Experiments were performed in two technical and six biological replicates.

Cell lysis for RNA/protein extraction

For RNA extractions, neurons were rapidly washed twice with 1X PBS and lysed in 350 µl of cold RLT buffer (Qiagen) with 1% β-mercaptoethanol and collected immediately on ice. RNA sequencing samples were rapidly transferred and stored at -80°C until all samples were collected. For protein extractions, cells were rapidly washed twice with 1X PBS and lysed in 100 µl of RIPA buffer freshly supplemented with protease and phosphatase inhibitors (50 mM Tris-HCl, 150 mM sodium chloride, 1 mM EDTA, 1% triton X-100, 0.2% sodium deoxycholate supplemented with: 1.5 mM aprotinin, 100 mM 1-10 phenantroline, 100 mM 6-aminohexanoic acid, 1% protease inhibitor cocktail (Sigma), 1% phosphatase inhibitor cocktail (Sigma)). Lysates were kept on ice for 30 minutes with brief vortexing every 5 minutes. Samples were then centrifuged at 14000g for 10 minutes and supernatant was transferred to a clean tube. Samples were aliquoted and stored at -80°C until used for western blotting.

Immunoprecipitation

For immunoprecipitation, cells or tissue were lysed in freshly made IP lysis buffer (20 mM Tris-HCl, 150 mM NaCl, 1mM EDTA, 1% Triton X, 10 mM NaF, 1mM Na3VO4,1% protease inhibitor cocktail (Sigma), 1% phosphatase inhibitor cocktail (Sigma)). 10 µl of Protein G Sepharose beads were washed twice with 500 µl of cold 1X PBS by centrifugation (2000g, 2 min, 4°C). In parallel, tissue or cell-lysate samples were centrifuged (14000g, 10 min, 4°C). Sample supernatant was pre-cleared with the washed beads for 30 min at 4°C under constant rotation. Beads and non-specifically bound proteins were precipitated by centrifugation (2000g, 2 min, 4°C). 10% of sample supernatant was put aside and saved to be used as INPUT control. The remaining 90% of the supernatant was used for immunoprecipitation and added to 20 µl of pre-washed Protein G Sepharose beads with 2 µl of antibody of interest. After a 2-hour incubation at 4°C with constant rotation, samples were centrifuged (2000g, 2 min, 4°C) and washed with lysis buffer (3X 2000g, 2min, 4°C). Finally, samples were eluted in LDS buffer and incubated for 10 min at 70°C). Finally, the beads were removed by centrifugation (2000g, 5 min, RT). Samples were stored at -80°C until analysed by western blot. The

antibodies used for co-IP were anti-MYC (MA1-980 mouse monoclonal, Thermo Fisher), anti-KPNA1 (18137-1-AP rabbit polyclonal, Proteintech) and anti-PCDH19 (A304-648A rabbit polyclonal, Bethyl).

Western blotting

Protein lysates were prepared by addition of LDS buffer and 10% 0.5 M DTT, and boiled at 70°C for 10 min. Samples were then centrifuged at 14000 g for 10 min and loaded onto a NuPAGE Novex 4-12% Bis-Tris gel (Novex Life Technologies, WC1020) and run at 120 V for 90 minutes. Proteins were transferred to a nitrocellulose membrane with a 0.2 µm pore size (GE Healthcare Life Sciences, 10600001) by wet transfer at 100 V for 120 minutes. Membranes were incubated shaking for 1 hour at RT with 4% blocking solution (5% milk powder (BioRad) in TBS-T). Primary antibody incubation was done overnight at 4°C shaking. The following day, membranes were washed 3 times for 10 minutes in TBS-T and then incubated for 1 hour at RT with the appropriate secondary antibody (in 5% milk powder in TBS-T blocking). Membranes were washed again 3 times for 10 minutes in TBS-T. Blots were finally developed with 1 ml of WesternBright ECL substrate (Advansta) and imaged with a ChemiDoc XRS+ (BioRad), using the Image Lab software.

For western blot analysis of tissue samples, the protein concentration of each sample was measured using the Micro BCA™ Protein Assay Kit (Thermo Fisher), following the manufacturer's instructions. Colorimetric intensity was measuring using a FLOUstar Omega microplate reader (BMG Labtech). The samples were then diluted in lysis buffer to reach a concentration of 40 µg which was then used for western blotting as described above.

Primary antibodies used for western blot include: anti-PCDH19 C-terminal (1:1000, A304-648A rabbit polyclonal, Bethyl), anti PCDH19 N-terminal (1:1000, orb312580, rabbit polyclonal, Biorbyt); anti-N-Cadherin (1:1000, 33-3900 mouse monoclonal, clone 3B9, Thermo Fisher); anti-ADAM10 (1:1000, ab1997 rabbit polyclonal, Abcam); anti-Pan-Cadherin (1:1000, ab6529 rabbit polyclonal, Abcam); anti-HA (1:2000, ROHAHA rat polyclonal, clone 3F10, Roche); anti-MYC (1:2000, MA1-980 mouse monoclonal, Thermo Fisher); anti-Histone H3 (1:5000, ab1792, rabbit polyclonal, Abcam); anti-β-Actin (1:2000, ab8226 mouse monoclonal, Abcam) and anti-αTubulin (1:2000, T5168 mouse monoclonal, Sigma). Secondary antibodies used for western blot include anti-Rabbit-HRP (1:20000, Promega W4011); anti-Mouse-HRP (1:20000, Promega W4021) and anti-Rat-HRP (1:20000, R&D systems HAF005).

Subcellular fractionation

Mouse embryonic fibroblast (MEF) cell lysates were processed using the Mem-PER™ Plus Membrane Protein Extraction Kit (Thermo Fisher, 89842) following the manufacturer's instructions.

IHC and ICC

Animals were injected with 100 µl of Euthatal (Merial, R02701A) and transcardially perfused with 30 ml of 1X PBS, followed by 30 ml of 4% PFA. Brains were postfixed in 4% PFA overnight at 4°C, then washed in 1X PBS the following day and stored at 4°C in the dark until sectioned. 100 µm P10 brain sections for endogenous targeting of PCDH19, or cells on glass coverslips, were washed in 1X PBS for a minimum of 3 times, followed by several washes in PBS 1X containing 0.25% triton X-100 (0.25% PBS-T). Sections, or cells were incubated at RT for at least 3 hours in BSA/blocking solution in 0.25% PBS-T, then incubated with the primary antibodies overnight at 4°C in the dark. The following day, sections or cells were washed, and incubated with appropriate fluorescently-conjugated secondary antibodies, washed, counterstained with DAPI (1:4000 in 1X PBS) and mounted with DAKO mounting media on glass slides. For immunostaining of P60 electroporated brains, 350 µm sections were permeabilized in PBS 1X and 0.25% PBS-T and blocked in 3% Donkey Serum and 4% Bovine Serum Albumin (BSA) for 5 hours. Brain slices were incubated with primary antibodies for 36 hours at 37 ^{o}C. After that time, sections were thoroughly washed with 0.25% PBS-T and incubated with the appropriate fluorescently conjugated secondary antibodies, washed and counterstained with DAPI (1:4000 in 1X PBS) and mounted with DAKO mounting media on glass slides.
Primary antibodies used for immunostaining included anti-HA (1:500, ROHAHA rat polyclonal, clone 3F10, Roche) and anti-GFP (1:2000, A10262 chicken polyclonal antibody, Thermo Fisher).
Secondary antibodies included: anti-chicken 488 (Thermo Fisher; A11039 Alexa Fluor 488 goat anti-chicken; 1:1000) and anti-chicken 488 (Thermofisher; A11039 Alexa Fluor 488 goat anti-chicken; 1:1000).

Neuronal differentiation of mESCs

E14 male mouse embryonic stem cells (mESCs) used in this study were kindly provided by Dr. Xinsheng Nan (Cardiff University). Differentiation into cortical-like neurons was done

following the protocol by (Bibel et al., 2004) (Bibel et al., 2007). Although E14 mESCs are feeder-independent, in some instances, feeder passaging was added to the differentiation protocol to improve their quality. 12-well plates were used for protein and RNA extraction and 4-well plates for transfections and immunocytochemistry. Cells were plated in a range between ~750,000 and ~$1.5*10^6$ cells/well, depending on downstream applications.

Genetic engineering of mESCs

E14 mESCs were passaged the day before nucleofection. On the day, they were trypsinized and $4*10^6$ cells were used for one round of nucleofection. In brief, cells were pelleted and resuspended in 100 µl of P3 transfection solution (82 µl Amaxa Buffer and 18 µl P3 supplement; Lonza) and 10 µl of DNA mix. The following amount of plasmids were used: 10 µg of the targeting construct (pZDRosa-floxedNeo-Pcdh19-CYTO-HA) and 1 µg each of the two zinc finger nuclease (ZFN) plasmids: pCMV-RosaR4 KKR mutations, containing the right ZFN (ZFN-R), and the pCMV-RosaL6 ELD mutations, containing the left ZFN-L (ZFN-L). Cells were nucleofected using the 4D-Amaxa Nucleofector X-unit (Lonza) and the CG104 programme. Immediately after nucleofection cells were plated at low density for antibiotic selection. For removal of the neomycin resistance cassette, 10 µg of the pCIG-CRE plasmid was nucleofected as described above. After ZFN targeting, nucleofected cells were suspended in 10 ml of ESC medium and plated at densities ranging between 0.625 and 2.5 ml/10 cm dish. Cells underwent a 10-day selection process with 250 µg/ml of G418 (Geneticin), with media changed every two days. After about 10 days, or when they were visible by the naked-eye, 100 colonies were manually picked. In brief, cells were incubated for a couple of minutes with 0.01% trypsin (0.05% trypsin, diluted in PBS) in order for colonies to detach from the plate but without dissociating. Colonies were then carefully transferred to individual wells in a 96-well plate, trypsinized with 0.05% trypsin, resuspended and transferred to a 24-well plate to grow. Clones were expanded for DNA and protein extraction and then frozen. For mESC subcloning, after nucleofection for removal of the selection cassette, cells were plated at a density of 300 cells/10 cm plate. 24 colonies originating from different clones were picked as described above. Once expanded, these clones were “reverse selected” to test out loss of antibiotic resistance.

mESC genotyping

Cells were pelleted, resuspended in 500 µl of cell lysis buffer (10 mM Tris, pH 8.0, 1 mM CaCl2; 100 mM NaCl; 0.5% SDS; 5 mg/mL proteinase K (Promega)) and incubated overnight at 50°C. The following day, 500 µl of 100% isopropanol and 50 µl of 3 M NaOAc were added to precipitate DNA. DNA was pelleted by centrifugation (15 minutes at top-speed), washed with 70% ethanol and resuspended in 30 µl of TE buffer (Qiagen). Clones were genotyped by PCR, using the long-range sequal prep PCR kit (Thermo Fisher) and primers ReverseR26OUT2 (5'arm genomic; 5'-CAAGCGGGTGGTGGGCAGGAATGCG-3'), Neo-pR2 (5' arm selection cassette; 5'-TCGGCAGGAGCAAGGTGAGATGAC-3'), ForwardR26OUT2 (3' arm genomic; 5'-ACCAGAAGAGGGCATCAGATCCCATTAC-3') and gen19-ICDF2 (3' arm intracellular domain; 5'-GCGTGAAGCGTCTGAAGGATATCGTTC-3').

Karyotyping

mESC clones to be karyotyped were incubated with demecolcine solution (0.1 µg/ml) for two hours in the incubator. Cells were then trypsinized, pelleted and washed by centrifugation in 1X PBS twice, and subsequently resuspended in 2 ml of 1X PBS and 6 ml of hypotonic 0.0375 M potassium chloride solution and incubated for 12 min at 37°C. Cells were then pelleted, supernatant removed and a 3:1 volume:volume ratio of cold methanol/acetic acid mixture (-20°C) was added dropwise. After a 20 min incubation at room temperature, cells were pelleted again, supernatant removed, and fresh methanol/acetic acid was added. Cells were centrifuged one last time, the supernatant was removed, this time leaving about 100 µl, in which the cells were resuspended. Finally, cells were dropped from about 20 cm height on glass slides. Slides were left to dry, stained with DAPI (1:4000 in ddH2O), coverslipped and imaged immediately. A minimum of 10 cells were imaged for each clone. Chromosomes were then counted using the ImageJ (Fiji) cell-counter plug-in.

RNA sequencing

RNA extraction was done with RNeasy Kit (Qiagen) in RNase-free conditions following the user's manual with DNase treatment (Qiagen). Quality control of the samples was done via Tapestation (Agilent Technologies) and RNA integrity number (RIN) was determined for all samples. Concentration of samples was measure by QUBIT. RNA sequencing was done at Cardiff University

Genomic Hub. Libraries were prepared following Illumina's TruSeq Stranded mRNA sample preparation guide. In brief, mRNA was purified from total RNA using poly-T oligos, mRNA was then fragmented into smaller fragments and random priming was used for cDNA synthesis. The sequencing was carried out on a Illumina Nextseq 500 platform with 4 cartridges PE (2x75bp) sequencing on highoutput 150 cycle V2.5 cartridges. 1% Phix was spiked into each run as per the Illumina recommendations. The samples were pooled to obtain equal reads for each sample with an aim of at least 44 M reads per sample. Sequencing was paired end. Quality control of sequencing run, such as QC content and sequence duplication was performed before downstream analysis. Paired end reads from Illumina sequencing were trimmed of adaptor sequences with Trim Galore and assessed for quality using FastQC, using default parameters. Reads were mapped to the mouse GRCm38 reference genome using STAR (Dobin et al., 2013) and counts were assigned to transcripts using featureCounts (Liao et al., 2014) with the GRCm38 Ensembl gene build GTF. Both the reference genome and GTF were downloaded from the Ensembl FTP site (http://www.ensembl.org/info/data/ftp/index.html/). Differential gene expression analyses used the DESeq2 package (Love et al., 2014), using the Benjamini-Hochberg correction for multiple testing. Differential gene splicing analyses used the DEXSeq package (Anders et al., 2012), (Reyes et al., 2013) also using the Benjamini-Hochberg correction for multiple testing.

R packages for plotting

All plotting of RNA sequencing data was done on R (v.4.02) via RStudio (v.1.2.1335).
Plotting was done using R package "ggplot2" (v.3.3.2). Over-representation analysis and Gene Set Enrichment analysis was done via "clusterProfiler" (v.3.16.1) (Yu et al., 2012).

Quantitative real-time PCR

For RNA extraction, samples were collected and protected with RNAlater (Thermo Fisher) at -80 C for RNA extraction, which was performed using RNeasy Mini Kit (Qiagen) followed by RNase-Free DNase set (Qiagen). Maxima First Strand cDNA Synthesis Kit was used to generate the cDNA template for quantitative real-time PCR (Thermo Fisher). RT-PCRs were carried out with Applied Biosystems StepOne Plus and analysed using the corresponding software StepOne Software Version 2.0 (Applied Biosystems). Quantification was performed using a standard curve. The primers used

included *Erbb4*-fw (5'-CAAAGCCAACGTGGAGTTCATGG-3'), *Erbb4*-rv (5'-CTGCGTAACCAACTGGATAGTGG-3'), *Lhx2*-fw (5'-GATGCCAAGGACTTGAAGCAGC-3'), *Lhx2*-rv (5'-TTCCTGCCGTAAAAGGTTGCGC-3'), *Zic1*-m-fw (5'-TTTCCTGGCTGCGGCAAGGTTT-3') and *Zic1*-m-rv (5'-ACGTGCATGTGCTTCTTGCGGT-3').

In utero **electroporation**

For electroporations plug checking was performed, with noon of the day the plug was found considered as E0.5. Timed-pregnant females were deeply anesthetized with isoflurane and maintained in 2% isoflurane during the surgery. The abdominal cavity was opened, and the uterine horns were exposed. Then the DNA solution was injected into the lateral ventricle of the embryos through the uterus wall using pulled capillaries (PC-10, Digitimer). Embryos were electroporated at E15.5 by applying electric pulses (50V; 50ms on/950ms off/5 pulses) with an electric stimulator (BTX Electroporator ECM 830 (Harvard Apparatus)) using round electrodes (CUY650P5, NepaGene). DNA was diluted in 1X TE and coloured with 0.5% Fast Green (Sigma Aldrich). For the targeting of endogenous PCDH19, embryos were electroporated with the following combination of plasmids: pPB (0.5 µg/µl), pPB-CAG-MbEGFP (1 µg/µl), pPB-CAG-EGFP (1 µg/µl), pX330sgRNA#2 (1 µg/µl) and pLeakless-III-19-HA (2 µg/µl). For PCDH19-ICD overexpression, the plasmids used were pCIG and pCIG-19ICD-HA at a concentration of 1µg/ul.

Microscopy

Brain sections or cells were imaged on a confocal microscope (Carl Zeiss, LSM 780) with the Zen Black software (version 2.0, Carl Zeiss). For reconstruction of the neuronal morphology, 1 µm spaced Z-stack tiles, spanning the whole neuron, were taken with a 40X water-immersion objective. For spine analysis, representative segments of secondary order apical or basal dendrites belonging to the previously imaged neurons, were imaged with a 63X oil-immersion objective, as 1 µm spaced Z-stacks. Images of cultured cells (293HEKs, HeLa cells and mESC-derived neurons) were also taken with a 63X oil-immersion objective, as 1 µm spaced Z-stacks.

Image Analysis

Densitometric analysis of western blots was done using Image Lab (v.6.0.1) (BioRad). Lanes and bands were drawn in the software and adjusted volume intensity of each band was extracted. When calculating proteolytic fragments, full-length protein and fragment band intensity were detected on the same blot but using different exposures to avoid saturation. Intensity of the proteolytic fragment was always calculated as a ratio of the full-length protein.

Neuronal tracing analysis was done using the Fiji plugin SNT (Arshadi et al., 2021). Spines were counted manually, and dendrite was traced with SNT to determine length and calculate spines/20 μm.

Experimental Design and Statistical Analysis

Statistical analysis was carried out on GraphPad Prism (version 10.0.2). Shapiro-Wilk test was used to test for normality of the data. Data sets that passed the normality test ($P > 0.05$) were analysed with two-tailed unpaired Student's t-test when comparing two groups, or one-way ANOVA, followed by Tukey's correction for multiple comparisons if more than 2 groups were compared. For data sets that failed the normality test, the non-parametric Mann Whitney test was performed instead to compare between two samples (none of the data sets used for multiple comparisons failed the normality test). The only exception was the luciferase assay, where due to experimental conditions the variability between results obtained from the different experimental repeats was very high, so it was decided to normalize the data to one of the conditions before statistical analysis. Because one of the samples had all its values as 1 and had no variance, it was deemed more appropriate to carry out a one sample, two-tailed Student's t-test against a theoretical mean of 1 for those conditions that met the normality requirement, and the non-parametric Wilcoxon signed rank test against a theoretical median of 1 for those that didn't. No multiple comparisons between samples were carried out in this case. Kernel density analysis was performed using the R density base function with a standard gaussian fit and a bandwidth of 1. For the migration analysis, a histogram distribution of the distance of each electroporated neuron to the top of the cortical plate was created first, using 50 μm bins and combining all neurons from each condition (pCIG: 7 brains, 1895 neurons; pCIG-19ICD-HA: 11 brains, 3045 neurons). Next, a Kolmogorov-Smirnov test was run between the two histograms. For spine density analysis, segments of 1-5 basal and apical dendrites were analysed per neuron and values were averaged, so that n represents individual neurons and not individual dendrites.

Data are displayed as mean ± SEM in figures 1-7. However, in figure 1 data have been normalized to the values of one of the conditions for ease of visualization, even if the statistical analyses were performed with non-normalized data as described above.

RESULTS

Protocadherin 19 can be proteolytically cleaved

Given the interaction of PCDH19 with a nuclear protein (Pham et al., 2017), we theorized that PCDH19 could be proteolytically processed at the membrane to release a cytoplasmic fragment, as has been described for other cadherin family members. For PCDH19, processing would give rise to two fragments, slightly above and below 50-55 kDa if the proteolytic cascade matches the process described for similar adhesion molecules (CAMs) (Fig. 1A). CAM processing usually happens via a two-step process (Lichtenthaler et al., 2018). First, the extracellular domain is cleaved by a sheddase. This step releases a fragment into the extracellular space with the potential to act on neighbouring cells (Martín-de-Saavedra et al., 2022). The membrane-bound cytoplasmic domain generated by the first proteolytic event is then recognized by a second protease and is subjected to regulated intramembrane proteolysis (RIP). This second cut releases a soluble fragment into the cell cytoplasm that can sometimes translocate into the nucleus, providing a membrane (or synapse) to nucleus signalling pathway. To investigate if PCDH19 could be cleaved at all, we first generated a fusion protein of PCDH19 with the Gal4DBD-VP16 transactivation domain and performed a cleavage luciferase reporter assay in HEK293 cells (Fig. 1B) (Karlström et al., 2002; May et al., 2002). In this experiment, a plasmid expressing a C-terminal PCDH19-Gal4DBD-VP16 fusion was co-transfected with a reporter plasmid that contains upstream activating sequences (UAS) driving the expression of firefly luciferase. The Gal4 DNA binding domain fragment of the fusion protein will recognize the UAS sequences in the reporter plasmid and the VP16 fragment will activate the transcription of the luciferase gene. However, because PCDH19 is a membrane protein, the Gal4-VP16 fusion is sequestered at the membrane unless PCDH19 is proteolytically processed to release its cytoplasmic fragment. For this experiment we used the uncleavable IFNaR1 construct as negative control and the constitutively cleaved IFNaR2 as positive control (Sachse et al., 2019). Our results revealed a significant increase in luciferase activity when the cells were transfected with either the positive control or with PCDH19-Gal4-VP16 (IFNaR2 Ctrl: 144.97 ± 19.43, p = 0.0007; PCDH19-FL: 854.29 ±

64.4, $p < 0.0001$; values normalized to IFNaR1 Ctrl, one sample two-tailed Student's t-test, n = 6; Fig. 1C), therefore confirming that PCDH19 undergoes proteolytic processing.

Protocadherin 19 is proteolytically processed in cortical neurons, but not by ADAM10

Our luciferase assay results confirmed that PCDH19 can be proteolytically cleaved in HEK293 cells, suggesting that a similar process could take place in neurons. To address this question, we turned to ESC-derived cortical-like neurons, obtained following an established protocol that yields a highly pure (95%) population of these cells (Bibel et al., 2007). Treatment with ionomycin (a calcium ionophore previously described to increase proteolytic processing of cadherin family members, (Reiss et al., 2005; Marambaud et al., 2002)) greatly increased the intensity of two smaller bands above and below 50 kDa, which match the size of the predicted membrane bound CTF1 and soluble CTF2 fragments (Fig. 1D). These results demonstrated that PCDH19 undergoes proteolytic processing in neurons and that the main product of that cleavage is the CTF2 fragment of about 45 kDa.

Because ADAM10 functions as sheddase for several members of the cadherin superfamily (Maretzky et al., 2005; Reiss et al., 2005, 2006; Bouillot et al., 2011), we hypothesized that PCDH19 might also be cleaved by this protease. Therefore, we set out to explore this possibility using the ADAM10 specific inhibitor GI254023X in ESC-derived cortical-like neurons. However, a one-hour treatment with GI254023X before ionomycin addition did not reduce the intensity of the CTF1 and CTF2 bands (CTF1, Ctrl: 0.3 ± 0.07, 10' IM: 1.32 ± 0.13, 1h GI25X + 10' IM: 1.35 ± 0.22; n = 3; one way ANOVA, $F(2,6) = 14.84$, $p = 0.0048$; CTF2, Ctrl: 0.0005 ± 0, 10' IM: 0.24 ± 0.03, 1h GI25X + 10' IM : 0.2 ± 0.08; n = 3; one way ANOVA, $F(2,6) = 6.905$, $p = 0.0278$; Fig. 1D). To confirm that our treatment was effectively inhibiting ADAM10, we blotted the same lysates with an antibody against CDH2, which revealed a significant decrease in the intensity of its 37 kDa CTF band, confirming ADAM10 inhibition and a lack of involvement of ADAM10 in PCDH19 processing in cortical-like ESC-derived neurons (Ctrl: 0.07 ± 0.02, 10' IM: 1.97 ± 0.52, 1h GI25X + 10' IM: 0.23 ± 0.16; n = 3; one way ANOVA, $F(2,6) = 11.30$, $p = 0.0092$; Fig. 1E). Given this unexpected result, we expanded our analysis by using two further protease inhibitors: MK-8931 (or Verubecestat), and BB-94 (or Batimastat). Whereas treatment with MK-8931 did not have any effect on CTF1 or CTF2, ruling out the involvement of BACE1 or 2, BB-94 significantly decreased CTF1 intensity without affecting CTF2 (CTF1, Ctrl: 0.3 ±

0.04, 10’ IM: 1.1 ± 0.12, 1h MK-8931 + 10’ IM: 1.19 ± 0.13; 1h BB94 + 10’ IM: 0.48 ± 0.02; n = 3; one way ANOVA, F(3,8) = 23.30, p = 0.0003; CTF2, Ctrl: 0.0007 ± 0, 10’ IM: 0.3 ± 0.005, 1h MK-8931 + 10’ IM: 0.28 ± 0.04; 1h BB94 + 10’ IM: 0.29 ± 0.01; n = 3; one way ANOVA, F(3,8) = 58, p < 0.0001; Fig. 1F). Because BB-94 is a broad-spectrum matrix metalloproteinase (MMP) and ADAM inhibitor, our results suggest that other MMPs or ADAMs are the main proteases processing PCDH19 in mESC-derived cortical neurons.

The second step in the processing of other cadherin family members is carried out by the gamma-secretase complex to release their intracellular domains (Marambaud et al., 2002, 2003; Haas et al., 2005; Hambsch et al., 2005; Uemura et al., 2006; Bonn et al., 2007; Bouillot et al., 2011). To investigate the involvement of γ-secretase in PCDH19 processing, we treated mESC-derived neurons for 16 hours with the γ-secretase inhibitor DAPT, which led to an accumulation of CTF1 (Fig. 1G) but had no significant effect on CTF2, confirming that CTF1 is a substrate for this protease. Interestingly, a similar treatment with the calpain inhibitor calpeptin triggered a reduction in CTF2, indicating a potential role for calpain in the processing of PCDH19 (CTF1, Ctrl: 0.05 ± 0.01; 16h DAPT: 0.22 ± 0.02; 16h Calpeptin: 0.14 ± 0.03; n = 3; one way ANOVA, F(2,6) = 13.19, p = 0.0064; CTF2, Ctrl: 0.06 ± 0.004; 16h DAPT: 0.08 ± 0.003; 16h Calpeptin: 0.06 ± 0.007; n = 3; one way ANOVA, F(2,6) = 5.5, p = 0.044; Fig. 1G).

Together, our results indicate that PCDH19 is proteolytically processed in cortical-like neurons by MMPs or ADAMs other than ADAM10, and that gamma secretase, and possibly other proteases as well, are involved in the second proteolytic step.

Protocadherin 19 processing is activity dependent

We sought to confirm that proteolytic processing of PCDH19 also happens in the cortex *in vivo*. Western blot analysis of PCDH19 expression in mouse embryonic forebrain (E11) and postnatal day 10 (P10) cortical and hippocampal lysates detected CTF1 and CTF2 bands in wild type (WT) tissue, but not in samples obtained from *Pcdh19* knockout (KO) mice (Fig. 1H), which instead displayed an additional band of ~30 kDa, probably reflecting residual expression from exons 4-6, which are still present in this KO model. Interestingly, the CTF1 and 2 bands were much stronger in postnatal than

in embryonic lysates (Fig. 1H), indicating that processing is a more common event in neurons than in progenitors, which are the predominant cell type in E11 forebrain. We hypothesized that this difference could be due, at least in part, to activity-dependent processing of PCDH19, since proteolytic processing of synaptic cell adhesion molecules in response to neuronal activity is a well-documented phenomenon. To test this idea, we treated mESC-derived neurons with NMDA (Fig. 1I), leading to a significant increase in the intensity of the CTF2 band. Pre-treatment with MK-801, a specific inhibitor of the NMDA receptor, abolished this increase, indicating that activation of the NMDA receptor is sufficient to trigger PCDH19 processing (Ctrl: 0.004 ± 0; 30' NMDA: 0.33 ± 0.05; 30' NMDA + MK-801: 0.02 ± 0.02; n = 3; one way ANOVA, $F(2,6) = 37.65$, $p = 0.0004$; Fig. 1I).

Our data thus indicate that PCDH19 proteolytic processing is a common event, taking place in HEK293 cells, in cortical-like mESC-derived neurons and, more importantly, in the cortex *in vivo.* Moreover, in neuronal cells, the processing is activity dependent, with an increase in processing in response to NMDA receptor activation.

PCDH19-ICD translocates to the nucleus

Since the intracellular domain (ICD) of PCDH19 contains a putative nuclear localization signal (NLS) (Fig. 1A), we hypothesized that the proteolytic processing described above would generate a soluble fragment capable of entering the nucleus. This hypothesis was first examined by investigating the subcellular localization of PCDH19 full length protein (PCDH19-FL) and its ICD in mESC-derived neurons transfected with C-terminally HA-tagged constructs and probed for the HA tag. Neurons transfected with PCDH19-FL-HA displayed a strong perinuclear signal, as expected by the overexpression of a membrane protein, but hardly, if any, signal inside the nucleus (Fig. 2A). In contrast, the HA signal in neurons transfected with PCDH19-ICD-HA was almost exclusively nuclear (Fig. 2B). The same nuclear localization was observed in cortical neurons *in vivo* after electroporation with the PCDH19-ICD-HA plasmid (Fig. 2C). However, the above experiments rely on protein overexpression, and we also wanted to investigate the subcellular localization of the endogenous protein. To circumvent the problem with existing antibodies, we decided to tag endogenous PCDH19 C-terminally with HA in cortical neurons by a combination of CRISPR-Cas9 targeting and *in utero* electroporation (Fig. 2D). We generated a targeting vector using the pLeaklessIII backbone and the

coding sequence of PCDH19 exon 6, with an HA-tag attached before the stop codon and flanked by homology arms. We then electroporated this targeting vector at E15.5, together with an sgRNA cloned into the pX330 plasmid and two EGFP reporters to identify the electroporated cells. Although the targeting efficiency was low, we could identify several positive cells in layer 2/3 of the cortex after staining with anti-HA antibodies. All of them shared the same pattern of endogenous PCDH19 localizing mainly in the cell soma and the beginning of the apical dendrite, with very little, if any, nuclear staining (Fig. 2D). The absence of nuclear signal was not surprising, as the proportion of endogenous processed protein is probably too low to be detected through immunostaining.

To visualize how processing leads to the nuclear translocation of the intracellular fragment, we turned to an *in vitro* system in which we could more easily manipulate the cells. We transfected HeLa cells with PCDH19-FL-HA and treated them with ionomycin. A 20 minute treatment elicited a significant increase in nuclear signal (19FL: 30.21 ± 3.01; 19FL + 20' IM: 47.02 ± 2.64; n = 15; unpaired t-test, $p = 0.0002$; Fig. 2E), corroborating processing of PCDH19 and nuclear translocation of PCDH19-ICD. Further support for the nuclear translocation of PCDH19-ICD was obtained by blotting membrane- and cytoplasm/nucleus-enriched fractions of MEF protein lysates against PCDH19 (Fig. 2F). This experiment showed that the full-length protein and CTF1 are more prominent in the membrane fraction, whereas CTF2 is present in the cytoplasm/nucleus of the cell.

Our results thus confirm that the intracellular domain of PCDH19 adopts a nuclear localization when expressed on its own, but also when generated through proteolytic processing of the full-length protein.

Importins mediate the nuclear translocation of PCDH19-ICD

The presence of a predicted NLS indicates that the nuclear import of PCDH19-ICD might be mediated by the classical pathway involving importin dimers (Lu et al., 2021). To test whether PCDH19 interacts with importins, we carried out co-immunoprecipitation experiments with PCDH19 and importin subunit alpha 5 (KPNA1) (Fig. 3A). The interaction with PCDH19-FL-HA was weaker than with PCDH19-ICD-HA, suggesting that anchorage to the plasma membrane decreases the probability of interaction between the two proteins. To verify that this interaction is mediated by the predicted bipartite NLS (aa

762 to 780: “KRIAEYSYGHQKKSSKKKK”) and that the NLS is functional, we mutated its last four basic residues from “KKKK” to “AAAA” in the PCDH19-ICD-HA construct. As expected, expression of this construct in HeLa cells resulted in a significant reduction in nuclear signal ratio compared to non-mutated PCDH19-ICD-HA (19ICD: 82.17 ± 2.84; $19ICD_{(NLSmut)}$: 53.62 ± 3.51, n = 15; Mann-Whitney, $p < 0.0001$; Fig. 3B). Finally, we verified the interaction between PCDH19 and KPNA1 *in vivo*, by co-immunoprecipitation using P10 cortical lysates (Fig. 3C). Therefore, our data show that processing of PCDH19 generates a soluble cytoplasmic fragment with a functional NLS that is recognized by importins for nuclear transport.

Constitutive expression of PCDH19 ICD alters the expression of genes involved in neuronal differentiation.

Our results indicate that proteolytic processing of PCDH19 produces a soluble ICD fragment that can enter the nucleus, suggesting a potential role in gene regulatory function for this protein. However, although PCDH19 is known to regulate expression of immediate early genes (Gerosa et al., 2022), it is still unknown which impact PCDH19-ICD has on the transcriptional landscape of neurons. To address this question and to examine the potential gene regulatory function of PCDH19-ICD in neuronal cells, we generated a transgenic mESC line with constitutive expression of an HA-tagged cytoplasmic domain from the *Rosa26* locus in addition to the endogenous gene (Fig. 4A). Targeting of the *Rosa26* locus in E14 mESCs was carried out using zinc finger nucleases (Perez-Pinera et al., 2012) and positive clones were selected via antibiotic resistance (Fig. 4B). After a second nucleofection to remove the selection cassette, constitutive expression of the cytoplasmic domain of PCDH19 was confirmed via western blot (Fig. 4B, C). Clones selected for further analysis were karyotyped to ensure correct chromosomal numbers. The mESC line constitutively expressing PCDH19 cytoplasmic domain (19ICD-OE) showed similar proliferation rates as WT mESCs and could be successfully differentiated into cortical-like neurons (Fig. 4D). Bulk RNAseq analysis was then performed with samples obtained from three independent differentiations of control and 19ICD-OE mESC-derived neurons at DIV8 and DIV12, which confirmed a moderate increase in the expression of *Pcdh19* (about 1.3-fold at both stages) and, in particular, of transcripts corresponding to its intracellular domain (Fig. 4E). Principal component analysis (PCA) showed that PC1 accounted for 31% of the variance and mainly separated WT from 19ICD-OE samples, whereas PC2 accounted for

25% of the variance and separated DIV8 from DIV12 samples (Fig. 4F). Hierarchical clustering of samples confirmed the separation between WT and 19ICD-OE and echoed the differences between DIV8 and DIV12, except for the first differentiation of WT mESCs, for which DIV8 and DIV12 samples clustered together (Fig. 4G). These results reflect the transcriptional changes associated with neuronal maturation (between DIV8 and DIV12) and suggest that constitutive expression of PCDH19-ICD alters the neuronal transcriptome.

To investigate specific effects of PCDH19-ICD overexpression on the neuronal transcriptional landscape, we carried out differential expression analysis at each time point (DIV8 and DIV12), comparing 19ICD-OE and WT neurons. Analysis with cutoffs of FDR < 0.001 and log2 fold > 0.58 identified 269 differentially expressed genes (DEGs) at DIV8 and 232 DEGs at DIV12 (Fig. 4H). Although at DIV8 there were slightly more downregulated than upregulated genes (143 vs 106), by DIV12 that trend had disappeared, with roughly equal numbers of genes changed in both directions (113 vs 115). A comparison between DIV8 and DIV12 DEGs revealed 134 common genes, representing 50% of DIV8 and 58% of DIV12 DEGs, respectively (Fig. 4H). In all cases, the direction of change was maintained, suggesting continuous regulation of those genes by PCDH19-ICD over the course of neuronal maturation. Verification of differential expression by RT-PCR was performed for several genes (*Zic1*, *Lhx2* and *Erbb4*) (Fig. 4I).

Insight into the types of genes and processes affected by the transcriptional changes was obtained by subjecting the identified DEGs to an over-representation analysis matching against gene ontology (GO) terms. Given the differences in the manual and algorithm-based assignment of genes to specific GO terms between platforms, we compared the results obtained with g:Profiler (Raudvere et al., 2019), ShinyGO (Ge et al., 2019) and Panther (Thomas et al., 2003; Mi et al., 2010). Among the top 15 GO terms for biological function at DIV8, four terms were shared between all three platforms: “neurogenesis” (average FDR across the three platforms (FDR_A)= 5.80E-14), “generation of neurons” (FDR_A = 5.80E-14), “neuron differentiation” (FDR_A = 8.07E-13) and “animal organ morphogenesis” (FDR_A = 7.44E-12) (Fig. 5A and Extended Data Table 5-1). In addition, another 9 terms were common for gProfiler and Panther, all related to developmental and differentiation processes, including “nervous system development” (g:Profiler FDR = 1.25E-24; Panther FDR = 1.40E-19). The ShinyGO

results were the most dissimilar, mainly because of the inclusion of several GO terms related to transcriptional regulation. However, they also included “neuron projection guidance” (FDR = 9.57E-07), “axon guidance” (FDR = 9.57E-07) and “cell morphogenesis involved in neuron differentiation” (FDR = 9.60E-07), suggesting that PCDH19-ICD broadly regulates expression of genes involved in various pathways related to neuronal morphogenesis. At DIV12, “neurogenesis” (FDR_A = 1.54E-06), “generation of neurons” (FDR_A = 5.22E-07) and “neuron differentiation” (FDR_A = 2.94E-06) were also significant across the three platforms, although only “neurogenesis” and “generation of neurons” figured among the top 15 most significant biological process GO terms in Panther, with broader terms related to differentiation and transcription ranking higher in gProfiler and ShinyGO (Fig. 5B and Extended Data Table 5-1). Ingenuity pathway analysis of diseases and functions of the differentially expressed genes produced similar results, with the function “differentiation of neurons” showing the lowest P-value at DIV8 ($P_{(DIV8)}$ = 6.4E-20) and the ninth lowest at DIV12 ($P_{(DIV12)}$ = 4.03E-13). Other related functions, such as “development of neurons” ($P_{(DIV8)}$ = 1.61E-09; $P_{(DIV12)}$ = 8.42E-06), “neuritogenesis” ($P_{(DIV8)}$ = 2.74E-06; $P_{(DIV12)}$ = 1.07E-04) and “guidance of axons” ($P_{(DIV8)}$ = 8.12E-09; $P_{(DIV12)}$ = 9.54E-07) also displayed highly significant P values at DIV8 and DIV12. Interestingly, the z-score associated with the pathway “differentiation of neurons” reached the threshold to be predicted as decreased at DIV8 (z-score -2.318), although not at DIV12 (z-score -1.234). Furthermore, two functions related to synaptic function, “synaptic transmission” ($P_{(DIV8)}$ = 6.31E-06; z-score -2.158) and “neurotransmission” ($P_{(DIV8)}$ = 3.65E-05; z-score -2.359) were also predicted to be decreased at DIV8, indicating that PCHD19-ICD might negatively regulate some of those processes, at least during early stages, or that compensatory mechanisms emerge as development progresses. Involvement of PCDH19-ICD in neuronal morphogenesis and differentiation was further supported by the analysis of cellular components, where a majority of significant GO terms were related to neuronal projections and synapses at DIV8 (Fig. 5C).

With respect to individual genes, many of the DEGs linked to the GO terms “neuronal differentiation”, “generation of neurons” and “neurogenesis” were shared between the two stages, representing about 54% at DIV8 and 77% at DIV12 (Fig. 5D), further supporting the hypothesis of continuous regulation by PCDH19-ICD. Interestingly, all the DEGs linked to the GO term “neuronal differentiation” were included within the “generation of neurons” and “neurogenesis” gene sets both at DIV8 and DIV12

(Fig. 5E). However, given that by DIV8/DIV12 most cells in the cultures are of neuronal nature, we proceeded to investigate the molecular function of the genes assigned to the GO term "neuronal differentiation". At DIV8, about half of those DEGs were transcription factors, mainly of the homeodomain (*Barhl2, Evx1*, *Hoxa1, Hoxc8, Irx1, Irx2, Irx4, Meis1, Onecut2, Vsx2*, *Phoxa2*, *Pax6*, *Pou4f3*, *Gbx2*, *Lhx2*, *Lhx4, Uncx* and *Barhl2*) and zinc finger (*Bcl11b*, *Bcl6*, *Casz1, Rest, Zic1* and *Zic2*) families (Fig. 5F), including known regulators of cortical neuronal fate and differentiation, such as *Pax6*, *Lhx2* and *Bcl11b* (also known as *Ctip2*). A series of transmembrane cell adhesion molecules and receptors, such as *Boc, Epha6, Erbb4, Fzd10, Gpr37, Kcnip2, Lrp4, Ltk, Nrp1, Nrp2, Pcdh15, Prtg, Rtn4rl1, Sipr1, Sdk2* and *Trpc6* also displayed differential expression (Fig. 5F), as did several secreted factors (*Bmp4, Bmp7, Lgi1, Ndnf, Ntn1 and Ptn*) (Fig. 5F). Results were similar at DIV12, with many of the DEGs associated with those three GO terms also encoding transcription factors and membrane proteins. Beyond those three GO:BP terms, and in concordance with the results of the cellular component analysis (GO:CC), several DEGs coded for synaptic proteins, including neurotransmitter receptors (*Chrna5, Gabrg2, Gabrg3, Glra3, Grik3, Grm3 and Grm8*), components of synaptic vesicles (*Rab3b, Synpr, Sv2b and Slc17a8*) and other synaptic membrane proteins (*Cacng5, Cdh9, Cnih3, Erbb4, Nrp1, Nrp2, Pcdh15 and Sdk2*).

Together, our results show that PCDH19-ICD broadly affects the neuronal transcriptome and, in particular, the expression of genes involved in the process of neuronal and synaptic differentiation.

Overexpression of PCDH19-ICD in upper layer cortical neurons does not impact neuronal numbers, positioning, or axonal targeting

Considering the results obtained in our transcriptomic analysis, with DEGs linked to GO terms related to different processes of neuronal differentiation, we decided to investigate the consequences of PCDH19-ICD overexpression *in vivo*, to better understand the roles that proteolytic processing of this cell adhesion protein plays in the cortex. To this end we carried out functional analyses using *in utero* electroporation at embryonic day E15.5 to target cortical layer 2/3, one of the main cortical populations known to express *Pcdh19* (Galindo-Riera et al., 2021). We electroporated control plasmid pCIG or pCIG-PCDH19-ICD-HA (abbreviated pCIG-19ICD-HA) and analyzed mature neurons at postnatal day P60 after immunostaining with anti-HA and anti-EGFP antibodies (Fig. 6A). As described above, PCDH19-ICD was mainly localized in the nucleus (Fig. 6A, see also Fig. 2C).

Although *Pcdh19* is not expressed in radial glia progenitors at E15.5, the stage at which we performed the electroporations, overexpression of its cytoplasmic domain in these cells could potentially interfere with the normal production of neurons. In addition, “neurogenesis” and “generation of neurons” were significant GO terms in our RNAseq analysis. Therefore, we first compared the total number of EGFP-expressing cells between pCIG and pCIG-19ICD-HA electroporated brains, as well as the cortical thickness of the electroporated areas to investigate a potential effect of PCDH19-ICD in this process. Since no differences were apparent between the two conditions (EP cells, pCIG: 271 ± 38, n = 7; pCIG-19ICD-HA: 277 ± 51, n = 11; unpaired t-test, $p = 0.933$; cortical thickness, pCIG: 1505.41 ± 213.31 µm, n = 7; pCIG-19ICD-HA: 1394.79 ± 135.99 µm, n = 11; unpaired t-test, $p = 0.6512$; Fig. 6B), our results suggest that expression of PCDH19-ICD at E15.5 does not have a major effect on neuronal production or survival, which would otherwise result in a significant decrease in the amount of electroporated neurons in all brains electroporated with the pCIG-19ICD-HA construct.

Another developmental process that could be impacted by PCDH19-ICD is neuronal migration. Although not part of the top 15 biological processes, the GO term “neuron migration” was significant across all three platforms and at both developmental stages in our RNAseq analysis ($FDR_{A(DIV8)}$ = 9.40E-04; $FDR_{A(DIV12)}$ = 1.77E-04). Therefore, we mapped the position and calculated the distance to the pial surface for every electroporated neuron and performed Kernel density analysis to model their respective distributions (Fig. 6C). No significant differences were found between the two conditions through statistical analysis (2-sample Kolmogorov-Smirnov test; D = 0.1622; P = 0.7154). These results suggest that overexpression of PCDH19-ICD does not impact radial migration of upper layer cortical neurons. Furthermore, because neuronal position is correlated with the timing of neuronal production and with neuronal fate, these data also support the previous observation that electroporation of pCIG-19ICD-HA does not significantly alter neurogenesis at this stage.

“Neuron projection guidance” and “axon guidance” were among the 15 most significant GO terms at DIV8 for ShinyGO, also reaching statistical significance at both ages across all three platforms ($FDR_{A(DIV8)}$ = 3.58E-07 and 3.56E-07; $FDR_{A(DIV12)}$ = 1.11E-05 and 1.12E-05, respectively), alongside terms like “axon development” ($FDR_{A(DIV8)}$ = 1.00E-06; $FDR_{A(DIV12)}$ = 6.6E-04) and “axonogenesis” ($FDR_{A(DIV8)}$ = 1.91E-06; $FDR_{A(DIV12)}$ = 2.17E-04). To determine if the transcriptional changes elicited by

PCDH19-ICD impact axonal formation or navigation *in vivo*, we next assessed the axonal projections of the electroporated neurons (Fig. 6D, E). Although the EGFP fluorescence intensity of pCIG-19ICD-HA targeted neurons is lower than that of control cells due to plasmid architecture, we could still follow their axons across the *corpus callosum* and into the contralateral hemisphere in both cases, with no evidence of misguided axons within the cortex or in other areas, such as the striatum. Hence, despite the dysregulation of genes related to the formation and guidance of axons in mESC-derived neurons, no obvious axonal defects were found *in vivo*.

Expression of PCDH19-ICD in cortical neurons reduces the number of spines without affecting neuronal morphology

After ruling out any major effects of PCDH19-ICD on axonal guidance, we next checked if the changes to the transcriptional landscape elicited by this fragment had an impact on overall neuronal morphology (Fig. 7A). To this end, we imaged and traced electroporated neurons to evaluate any potential changes in dendritic arborization (Fig. 7B). No differences were found in the width of the apical or basal dendritic arbors (apical, pCIG: 284.55 ± 33.99 μm, n = 11; pCIG-19ICD-HA: 266.29 ± 21.79 μm, n = 12; Mann-Whitney, p = 0.9279; basal, pCIG: 273.23 ± 25.74 μm, n = 11; pCIG-19ICD-HA: 261.59 ± 11.53 μm, n = 12; Mann-Whitney, p = 0.9759; Fig. 7C) nor in the total added length of dendrites of the different orders (order 1, pCIG: 635.63 ± 50.62 μm, n = 11; pCIG-19ICD-HA: 576.2 ± 88.5 μm, n = 12; independent t-test, p = 0.5755; order 2, pCIG: 1294.99 ± 106.45 μm, n = 11; pCIG-19ICD-HA: 1198.27 ± 107.49 μm, n = 12; independent t-test, p = 0.5305; order 3, pCIG: 1598.32 ± 185.51 μm, n = 11; pCIG-19ICD-HA: 1473.14 ± 210.04 μm, n = 12; independent t-test, p = 0.6621; order 4, pCIG: 667.7 ± 146.87 μm, n = 10; pCIG-19ICD-HA: 606.9 ± 116.48 μm, n = 11; independent t-test, p = 0.747; order 5, pCIG: 153.27 ± 50.88 μm, n = 7; pCIG-19ICD-HA: 287.68 ± 108.69 μm, n = 9, Mann-Whitney , p = 0.4874; Path lengths 6 to 8 could not be tested due to low numbers; Fig. 7D). Sholl analysis didn't show any other morphological differences between neurons electroporated with pCIG or with pCIG-19ICD-HA (Fig. 7E). These results, together with the lack of axonal phenotypes, suggest that the transcriptional changes elicited by PCDH19-ICD either do not directly affect neuronal morphology *in vivo*, or can be compensated during development, giving rise to morphologically unaltered neurons.

PCDH19 localizes at synapses and its proteolytic processing is activity dependent, pointing to a potential synapse to nucleus signaling pathway. In addition, at DIV8, terms like “chemical synaptic transmission” (FDR_A = 0.02), and “anterograde trans-synaptic signaling” (FDR_A = 0.02) were also significant across gProfiler, Panther and ShinyGO, and IPA analysis predicted the functions “synaptic transmission” and “neurotransmission” to be decreased. Furthermore, the top 10 most significant cellular component GO terms in all three platforms were mainly synaptic (Fig. 5C and Extended Data Table 5-1) and many DEGs encoded synaptic proteins. Because most excitatory synapses are located on dendritic spines, we hypothesized that PCDH19-ICD might impact differentiation processes related to spine formation or stabilization. To test this hypothesis, we quantified the number of spines in dendrites from pCIG and pCIG-19ICD-HA electroporated neurons and calculated the spine density. Interestingly, pCIG-19ICD-HA electroporated neurons showed a ~36% reduction in total spine density (pCIG: 17.16 ± 0.62 spines/20μm, n = 16; pCIG-19ICD-HA: 11.04 ± 0.49 spines/20μm, n = 12; Mann-Whitney, $p < 0.0001$, Fig. 7G). This reduction was slightly more pronounced across basal (~40%) than apical (~32%) spines (apical, pCIG: 16.36 ± 0.49 spines/20μm, n = 15; pCIG-19ICD-HA: 11.20 ± 0.61 spines/20μm, n = 11; independent t-test, p = 6.75E-07; Fig. 7H; basal, pCIG: 17.91 ± 0.87 spines/20μm, n = 16; pCIG-19ICD-HA: 10.87 ± 0.53 spines/20μm, n = 12; Mann-Whitney, $p < 0.0001$; Fig. 7I). Our results demonstrate that upper layer cortical neurons overexpressing PCDH19-ICD *in vivo* have fewer spines on their dendrites, pointing to a role of this fragment, and thus of the proteolytic processing of PCDH19, in the regulation of spine density.

DISCUSSION

PCDH19 is a cell adhesion protein mutated in a form of epileptic encephalopathy (Dibbens et al., 2008), but the way in which it contributes to the disorder is complex and currently not understood. We have investigated here non adhesive functions of PCDH19, and we provide evidence that its intracellular domain regulates expression of genes involved in neuronal differentiation and controls spine density in upper layer cortical excitatory neurons. Our biochemical experiments demonstrate that proteolytic cleavage of PCDH19, which is activity dependent in neurons, generates a soluble fragment that interacts with importins to be transported into the nucleus. Using RNAseq, we further show that the intracellular domain of PCDH19 elicits broad transcriptional changes associated with neuronal differentiation processes in mESC-derived neurons. Our *in vivo* functional analysis indicates

that overexpression of PCDH19-ICD in layer 2/3 cortical neurons does not affect overall neuronal numbers or position, neuronal morphology or axonal development, but leads to a reduction in apical and basal spine density. Our data thus point to a new way in which PCDH19 might contribute to the pathophysiology of the epileptic encephalopathy it is associated with.

Proteolytic processing has been described for members of different cell adhesion families, including neuroligins, NCAM and cadherins (Lee and Ch'ng, 2020). Processed cadherins include CDH1, CDH2, PCDH12 and the clustered alpha and γ-protocadherins, and in all cases ADAM10 and γ-secretase play a role in the proteolytic steps (Marambaud et al., 2002, 2003; Haas et al., 2005; Hambsch et al., 2005; Maretzky et al., 2005; Reiss et al., 2005, 2006; Uemura et al., 2006; Bonn et al., 2007; Bouillot et al., 2011). A similar scenario has recently been described for PCDH19 in cultured hippocampal neurons (Gerosa et al., 2022), again involving ADAM10 and, possibly, γ-secretase. Our results confirm the proteolytic cleavage of PCDH19 and its activity dependence in neuronal cells but seem to rule out a major sheddase role for ADAM10 in cortical-like neurons. Instead, other metalloproteases or ADAMs are likely to be involved in these cells. With regards to the second proteolytic step, our data also indicate the involvement of additional proteases, such as calpain, in addition to γ-secretase. Thus, the specific mechanism of PCDH19 processing might be cell type dependent, or cuts by different proteases might by triggered by specific stimuli depending on the cellular context.

Soluble fragments generated by proteolytic processing of membrane proteins can display further biological functions inside the cell. Interestingly, nuclear translocation of the processed fragments has been described for several CAMs, like ERBB4 (Allison et al., 2011), L1 (Minguez et al., 2020) or DSCAM/DSCAML (Sachse et al., 2019). Within the cadherin superfamily, the ICDs of CDH2 and the γ-protocadherins also localize to the nucleus, and the nuclear functions of these fragments have been characterized to some extent. CDH2-ICD binds to CBP, leading to its degradation and a reduction in CREB dependent transcriptional activity (Marambaud et al., 2003), while γ-protocadherin ICD leads to an increase in γ-protocadherin expression, indicative of an autoregulatory loop (Hambsch et al., 2005). However, genome wide analyses of the changes that nuclear ICDs elicit at the transcriptional level are still scarce and include DSCAM and DSCAML in HEK293 cells (Sachse et al., 2019), and ERBB4 using microarrays in rat cultured hippocampal neurons (Allison et al., 2011), but no such data

are available for members of the cadherin superfamily. We have evaluated here the alterations in the transcriptional landscape of mESC-derived neurons constitutively expressing PCDH19-ICD and have found broad changes in gene expression programs relevant for neuronal differentiation. Given the expression profile of *Pcdh19*, which peaks at about postnatal day 7 in the mouse cortex and is then maintained throughout adulthood, and the fact that proteolytic processing of PCDH19 is activity dependent, our results point to a role of this protein in the regulation of neuronal differentiation in response to neuronal activity.

Assessing the *in vivo* relevance of CAM proteolytic events is challenging, not least because of the lack of conserved protease recognition sequences that would facilitate the generation of cleavage defective versions. Only recently has a CDH2 cleavage resistant mouse model been characterized (Asada-Utsugi et al., 2021) that displays spine and synapse anomalies in the hippocampus and enhanced spatial memory. Because the specific sites at which PCDH19 is processed are currently unknown, our approach to evaluate the *in vivo* functions of PCDH19-ICD has been the opposite, overexpressing it in upper layer cortical neurons to evaluate the consequences of excessive processed fragment. This approach has allowed us to identify a role for PCDH19-ICD in the regulation of spine number, with continuous expression leading to a reduction in apical and basal spine density. These results could reflect an involvement of PCDH19 in synaptic homeostasis, wherein neuronal activity would trigger its proteolytic processing and the resulting fragment would then regulate synaptic numbers through a nuclear signaling and transcriptional pathway. Because PCDH19 and CDH2 are known to interact (Biswas et al., 2010; Emond et al., 2011), CDH2 is also processed in response to neuronal activity (Marambaud et al., 2003), and cleavage resistant CDH2 leads to increased spine density (Asada-Utsugi et al., 2021), it will be interesting to investigate in the future if and how these two cadherins cooperate to maintain optimal spine density in excitatory neurons.

One limitation of our study is that overexpression of PCDH19-ICD is more akin to a gain of function scenario that might not match the consequences of mosaic loss of function of the protein in patients. However, in order to elucidate the pathophysiological underpinnings of the epileptic encephalopathy caused by mutations in PCDH19, it is necessary to understand the different functions of this protein, including the less studied, non-adhesive, nuclear roles as the one described here that might offer new

insights into the molecular mechanisms at play in this disorder. In this regard, it will be interesting to investigate the *in vivo* roles of PCDH19-ICD both at earlier stages and after neuronal stimulation to evaluate relative contributions of PCDH19 to spine formation/maintenance during development and to spine and synaptic homeostasis in adulthood.

Data availability: The complete RNAseq data are available in the GEO repository.

Conflict of interest statement: The authors have no relevant financial or non-financial interests to disclose.

Acknowledgements: This work was supported by the PCDH19 Alliance (research grant to I.M-G.), the Life Science Research Network Wales, an initiative funded through the Welsh Government's Ser Cymru program (initial fellowship to I.M-G.), the Wellcome Trust (Seed Award 109643/Z/15/Z to I.M-G., fellowship 204021/Z/16/A to S.A.N., fellowship 220002/Z/19/Z to I.W.J.F.), and the Biotechnology and Biological Sciences Research Council (BBSRC) (grant BB/S002359/1 to I.M-G.). We would like to thank James Wilding for initial experiments that didn't make it into this manuscript and Rebecca Hughes for her participation in the cloning of PCDH19ICD(NLSmut)-HA and IPO5-myc. We would also like to thank Prof Yves Barde, Dr David Petrik and the members of their labs, as well as Prof Ulrich Mueller for their useful feedback during the completion of this work, and Dr Eva Porlán for her insightful comments on proteolytic processing analysis.

Author contributions: SAN, CG-S and IM-G designed research; SAN, IWJF, CLI-B, JF-B, ES and IM-G performed research; SAN, IWJF, CLI-B, ES and IM-G analyzed data; IM-G wrote the manuscript.

REFERENCES

Allison JG, Das PM, Ma J, Inglis FM, Jones FE (2011) The ERBB4 intracellular domain (4ICD) regulates NRG1-induced gene expression in hippocampal neurons. Neurosci Res 70:155–163.

Arshadi C, Günther U, Eddison M, Harrington KIS, Ferreira TA (2021) SNT: a unifying toolbox for quantification of neuronal anatomy. Nat Methods 18:374–377.

Asada-Utsugi M, Uemura K, Kubota M, Noda Y, Tashiro Y, Uemura TM, Yamakado H, Urushitani M, Takahashi R, Hattori S, Miyakawa T, Ageta-Ishihara N, Kobayashi K, Kinoshita M, Kinoshita A (2021) Mice with cleavage-resistant N-cadherin exhibit synapse anomaly in the hippocampus and outperformance in spatial learning tasks. Mol Brain 14:23.

Bassani S, Cwetsch AW, Gerosa L, Serratto GM, Folci A, Hall IF, Mazzanti M, Cancedda L, Passafaro M (2018) The female epilepsy protein PCDH19 is a new GABAAR binding partner that regulates GABAergic transmission as well as migration and morphological maturation of hippocampal neurons. Human Molecular Genetics 27:1027–1038.

Bibel M, Richter J, Lacroix E, Barde Y-A (2007) Generation of a defined and uniform population of CNS progenitors and neurons from mouse embryonic stem cells. Nature Protocols 2:1034–1043.

Bisogni AJ, Ghazanfar S, Williams EO, Marsh HM, Yang JY, Lin DM (2018) Tuning of delta-protocadherin adhesion through combinatorial diversity. eLife 7:400.

Biswas S, Emond MR, Jontes JD (2010) Protocadherin-19 and N-cadherin interact to control cell movements during anterior neurulation. The Journal of Cell Biology 191:1029–1041.

Bonn S, Seeburg PH, Schwarz MK (2007) Combinatorial expression of alpha- and gamma-protocadherins alters their presenilin-dependent processing. Molecular and Cellular Biology 27:4121–4132.

Bouillot S, Tillet E, Carmona G, Prandini M-H, Gauchez A-S, Hoffmann P, Alfaidy N, Cand F, Huber P (2011) Protocadherin-12 Cleavage Is a Regulated Process Mediated by ADAM10 Protein EVIDENCE OF SHEDDING UP-REGULATION IN PRE-ECLAMPSIA*. J Biol Chem 286:15195–15204.

Budzyński MA, Puustinen MC, Joutsen J, Sistonen L (2015) Uncoupling Stress-Inducible Phosphorylation of Heat Shock Factor 1 from Its Activation. Mol Cell Biol 35:2530–2540.

Cong L, Ran FA, Cox D, Lin S, Barretto R, Habib N, Hsu PD, Wu X, Jiang W, Marraffini LA, Zhang F (2013) Multiplex genome engineering using CRISPR/Cas systems. Science (New York, NY) 339:819–823.

Dalva MB, McClelland AC, Kayser MS (2007) Cell adhesion molecules: signalling functions at the synapse. Nat Rev Neurosci 8:206–220.

Dean C, Scholl FG, Choih J, DeMaria S, Berger J, Isacoff E, Scheiffele P (2003) Neurexin mediates the assembly of presynaptic terminals. Nat Neurosci 6:708–716.

Depienne C et al. (2009) Sporadic infantile epileptic encephalopathy caused by mutations in PCDH19 resembles Dravet syndrome but mainly affects females. Meisler MH, ed. PLoS Genetics 5:e1000381.

Dibbens LM et al. (2008) X-linked protocadherin 19 mutations cause female-limited epilepsy and cognitive impairment. Nature Genetics 40:776–781.

Emond MR, Biswas S, Blevins CJ, Jontes JD (2011) A complex of Protocadherin-19 and N-cadherin mediates a novel mechanism of cell adhesion. The Journal of Cell Biology 195:1115–1121.

Fièvre S, Carta M, Chamma I, Labrousse V, Thoumine O, Mulle C (2016) Molecular determinants for the strictly compartmentalized expression of kainate receptors in CA3 pyramidal cells. Nat Commun 7:12738.

Galindo-Riera N, Newbold SA, Sledziowska M, Llinares-Benadero C, Griffiths J, Mire E, Martinez-Garay I (2021) Cellular and behavioral characterization of Pcdh19 mutant mice: subtle molecular

changes, increased exploratory behavior and an impact of social environment. Eneuro 8:ENEURO.0510-20.2021.

Ge SX, Jung D, Yao R (2019) ShinyGO: a graphical enrichment tool for animals and plants. Bioinformatics 36:2628–2629.

Gerosa L, Mazzoleni S, Rusconi F, Longaretti A, Lewerissa E, Pelucchi S, Murru L, Giannelli SG, Broccoli V, Marcello E, Kasri NN, Battaglioli E, Passafaro M, Bassani S (2022) The epilepsy-associated protein PCDH19 undergoes NMDA receptor-dependent proteolytic cleavage and regulates the expression of immediate-early genes. Cell Reports 39:110857.

Haas IG, Frank M, Véron N, Kemler R (2005) Presenilin-dependent processing and nuclear function of gamma-protocadherins. The Journal of biological chemistry 280:9313–9319.

Hambsch B, Grinevich V, Seeburg PH, Schwarz MK (2005) {gamma}-Protocadherins, presenilin-mediated release of C-terminal fragment promotes locus expression. The Journal of biological chemistry 280:15888–15897.

Hayashi S, Inoue Y, Hattori S, Kaneko M, Shioi G, Miyakawa T, Takeichi M (2017) Loss of X-linked Protocadherin-19 differentially affects the behavior of heterozygous female and hemizygous male mice. Scientific reports 7:5801.

Hoshina N, Johnson-Venkatesh EM, Hoshina M, Umemori H (2021) Female-specific synaptic dysfunction and cognitive impairment in a mouse model of PCDH19 disorder. Science 372:eaaz3893.

Juberg RC, Hellman CD (1971) A new familial form of convulsive disorder and mental retardation limited to females. The Journal of pediatrics 79:726–732.

Karlström H, Bergman A, Lendahl U, Näslund J, Lundkvist J (2002) A Sensitive and Quantitative Assay for Measuring Cleavage of Presenilin Substrates*. J Biol Chem 277:6763–6766.

Lee YJ, Ch'ng TH (2020) RIP at the Synapse and the Role of Intracellular Domains in Neurons. Neuromol Med 22:1–24.

Lichtenthaler SF, Lemberg MK, Fluhrer R (2018) Proteolytic ectodomain shedding of membrane proteins in mammals—hardware, concepts, and recent developments. The EMBO Journal 37:e99456.

Lu J, Wu T, Zhang B, Liu S, Song W, Qiao J, Ruan H (2021) Types of nuclear localization signals and mechanisms of protein import into the nucleus. Cell Commun Signal Ccs 19:60.

Marambaud P, Shioi J, Serban G, Georgakopoulos A, Sarner S, Nagy V, Baki L, Wen P, Efthimiopoulos S, Shao Z, Wisniewski T, Robakis NK (2002) A presenilin-1/gamma-secretase cleavage releases the E-cadherin intracellular domain and regulates disassembly of adherens junctions. The EMBO Journal 21:1948–1956.

Marambaud P, Wen PH, Dutt A, Shioi J, Takashima A, Siman R, Robakis NK (2003) A CBP Binding Transcriptional Repressor Produced by the PS1/ϵ-Cleavage of N-Cadherin Is Inhibited by PS1 FAD Mutations. Cell 114:635–645.

Maretzky T, Reiss K, Ludwig A, Buchholz J, Scholz F, Proksch E, Strooper BD, Hartmann D, Saftig P (2005) ADAM10 mediates E-cadherin shedding and regulates epithelial cell-cell adhesion, migration, and beta-catenin translocation. Proceedings of the National Academy of Sciences of the United States of America 102:9182–9187.

Martín-de-Saavedra MD, Santos MD, Penzes P (2022) Intercellular signaling by ectodomain shedding at the synapse. Trends Neurosci 45:483–498.

Matsuda T, Cepko CL (2004) Electroporation and RNA interference in the rodent retina in vivo and in vitro. Proc National Acad Sci 101:16–22.

May P, Reddy YK, Herz J (2002) Proteolytic Processing of Low Density Lipoprotein Receptor-related Protein Mediates Regulated Release of Its Intracellular Domain*. J Biol Chem 277:18736–18743.

Mi H, Dong Q, Muruganujan A, Gaudet P, Lewis S, Thomas PD (2010) PANTHER version 7: improved phylogenetic trees, orthologs and collaboration with the Gene Ontology Consortium. Nucleic Acids Res 38:D204–D210.

Minguez MG, Wolters-Eisfeld G, Lutz D, Buck F, Schachner M, Kleene R (2020) The cell adhesion molecule L1 interacts with nuclear proteins via its intracellular domain. Faseb J 34:9869–9883.

Nagappan-Chettiar S, Johnson-Venkatesh EM, Umemori H (2017) Activity-dependent proteolytic cleavage of cell adhesion molecules regulates excitatory synaptic development and function. Neurosci Res 116:60–69.

Nishio H, Walsh MJ (2004) CCAAT displacement protein/cut homolog recruits G9a histone lysine methyltransferase to repress transcription. Proc Natl Acad Sci 101:11257–11262.

Nuriya M, Huganir RL (2006) Regulation of AMPA receptor trafficking by N-cadherin. J Neurochem 97:652–661.

Pederick DT, Richards KL, Piltz SG, Kumar R, Mincheva-Tasheva S, Mandelstam SA, Dale RC, Scheffer IE, Gécz J, Petrou S, Hughes JN, Thomas PQ (2018) Abnormal Cell Sorting Underlies the Unique X-Linked Inheritance of PCDH19 Epilepsy. Neuron 97:59-66.e5.

Peixoto RT, Kunz PA, Kwon H, Mabb AM, Sabatini BL, Philpot BD, Ehlers MD (2012) Transsynaptic Signaling by Activity-Dependent Cleavage of Neuroligin-1. Neuron 76:396–409.

Perez-Pinera P, Ousterout DG, Brown MT, Gersbach CA (2012) Gene targeting to the ROSA26 locus directed by engineered zinc finger nucleases. Nucleic Acids Res 40:3741–3752.

Pham DH, Tan CC, Homan CC, Kolc KL, Corbett MA, McAninch D, Fox AH, Thomas PQ, Kumar R, Gécz J (2017) Protocadherin 19 (PCDH19) interacts with paraspeckle protein NONO to co-regulate gene expression with estrogen receptor alpha (ERα). Human Molecular Genetics 26:2042–2052.

Prosser HM, Koike-Yusa H, Cooper JD, Law FC, Bradley A (2011) A resource of vectors and ES cells for targeted deletion of microRNAs in mice. Nat Biotechnol 29:840–845.

Raudvere U, Kolberg L, Kuzmin I, Arak T, Adler P, Peterson H, Vilo J (2019) g:Profiler: a web server for functional enrichment analysis and conversions of gene lists (2019 update). Nucleic Acids Res 47:W191–W198.

Reiss K, Maretzky T, Haas IG, Schulte M, Ludwig A, Frank M, Saftig P (2006) Regulated ADAM10-dependent ectodomain shedding of gamma-protocadherin C3 modulates cell-cell adhesion. The Journal of biological chemistry 281:21735–21744.

Reiss K, Maretzky T, Ludwig A, Tousseyn T, Strooper BD, Hartmann D, Saftig P (2005) ADAM10 cleavage of N-cadherin and regulation of cell–cell adhesion and β-catenin nuclear signalling. The EMBO Journal 24:742–752.

Sachse SM, Lievens S, Ribeiro LF, Dascenco D, Masschaele D, Horré K, Misbaer A, Vanderroost N, Smet ASD, Salta E, Erfurth M-L, Kise Y, Nebel S, Delm WV, Plaisance S, Tavernier J, Strooper BD, Wit J de, Schmucker D (2019) Nuclear import of the DSCAM-cytoplasmic domain drives signaling capable of inhibiting synapse formation. The EMBO Journal 38:e99669.

Saglietti L, Dequidt C, Kamieniarz K, Rousset M-C, Valnegri P, Thoumine O, Beretta F, Fagni L, Choquet D, Sala C, Sheng M, Passafaro M (2007) Extracellular interactions between GluR2 and N-cadherin in spine regulation. Neuron 54:461–477.

Servián-Morilla E, Robles-Lanuza E, Sánchez-Hidalgo AC, Camacho-Garcia RJ, Paez-Gomez JA, Mavillard F, Saura CA, Martinez-Mir A, Scholl FG (2018) Proteolytic Processing of Neurexins by Presenilins Sustains Synaptic Vesicle Release. J Neurosci 38:901–917.

Shinoe T, Goda Y (2015) Tuning synapses by proteolytic remodeling of the adhesive surface. Curr Opin Neurobiol 35:148–155.

Thalhammer A, Cingolani LA (2014) Cell adhesion and homeostatic synaptic plasticity. Neuropharmacology 78:23–30.

Thomas PD, Campbell MJ, Kejariwal A, Mi H, Karlak B, Daverman R, Diemer K, Muruganujan A, Narechania A (2003) PANTHER: A Library of Protein Families and Subfamilies Indexed by Function. Genome Res 13:2129–2141.

Tsunekawa Y, Terhune RK, Fujita I, Shitamukai A, Suetsugu T, Matsuzaki F (2016) Developing a de novo targeted knock-in method based on in utero electroporation into the mammalian brain. Development (Cambridge, England) 143:3216–3222.

Uemura K, Kihara T, Kuzuya A, Okawa K, Nishimoto T, Ninomiya H, Sugimoto H, Kinoshita A, Shimohama S (2006) Characterization of sequential N-cadherin cleavage by ADAM10 and PS1. Neuroscience letters 402:278–283.

Wit J de, Ghosh A (2016) Specification of synaptic connectivity by cell surface interactions. Nature Reviews Neuroscience 17:4–4.

Wolverton T, Lalande M (2001) Identification and characterization of three members of a novel subclass of protocadherins. Genomics 76:66–72.

FIGURE LEGENDS

Figure 1. PCDH19 is proteolytically processed in neurons in an activity dependent manner

A. Schematic of the PCDH19 protein indicating known domains and expected sizes after proteolytic processing. NTF: N-terminal fragment; CTF: C-terminal fragment; NLS: nuclear localization signal; CM: conserved motif; WIRS: WAVE interacting receptor sequence.

B. Illustration of the luciferase reporter assay to investigate PCDH19 processing.

C. Quantification (mean ± SEM) of the luciferase reporter assay in HEK293 cells. Results are shown normalized to the IFNaR1 (negative) control. IFNaR2 is a positive control known to be constitutively processed. (N=6)

D. Western blot detection (top) and quantification (bottom) of full length and processed PCDH19 in mESC-derived neurons under control, ionomycin or ionomycin + GI254023X treatments. (N=3)

E. Western blot detection (top) and quantification (bottom) of full length and processed CDH2 in mESC-derived neurons under control, ionomycin or ionomycin + GI254023X treatments. Same lysates as in panel A. (N=3)

F. Western blot detection (top) and quantification (bottom) of full length and processed PCDH19 in mESC-derived neurons under control, ionomycin, ionomycin + MK-8931 or ionomycin + BB-94 treatments. (N=3)

G. Western blot detection (top) and quantification (bottom) of full length and processed PCDH19 in mESC-derived neurons under control, DAPT and Calpeptin treatments. (N=3)

H. WB detection of PCDH19 in E11 cortical lysates and P10 cortical (CTX, C) and hippocampal (H) lysates of *Pcdh19* WT and KO mice.

I. Western blot detection (top) and quantification (bottom) of full length and processed PCDH19 in mESC-derived neurons under control, NMDA and NMDA + MK-801 treatments. (N=3)

Data information: (C) The ratio of Firefly to Renilla luciferase was used for quantification. (D-I) The ratio of CTF to FL band intensity was used for quantification. Data are normalized to IM treatment (D, E, F), control (G) or NMDA treatment (I) for ease of visualization and are presented as mean ± SEM. N: Biological replicate. Relevant p-values are indicated: *$p < 0.05$, **$p < 0.01$, ***$p < 0.001$, ****$P < 0.0001$. Statistical analysis: one-way ANOVA with Tukey's post-hoc test on non-normalized values.

Figure 2. PCDH19 ICD localizes to the nucleus after cleavage.

A, B. mESC-derived neurons transfected with PCDH19FL-HA (A) or PCDH19ICD-HA (B). Representative confocal images of transfected cells immunostained for HA. Nuclei are counterstained with DAPI. Scale bars: 20 µm (overview, top rows), 10 µm (inserts, bottom rows).

B. *In utero* electroporation to express PCDH19 ICD in upper layer cortical neurons. Strategy (top) and representative confocal images of a layer II/III neuron immunostained for HA for the control (pCIG) and 19ICD-HA conditions. Scale bar: 20 µm.

C. *In utero* electroporation to target endogenous PCDH19 with an HA tag. Strategy (top), targeting vector (middle) and representative confocal images of a layer II/III neuron immunostained for HA. Scale bars: 20 µm left panel, 10 µm middle and right panels.

D. Representative images of control and treated cells immunostained for HA (right) and quantification (left) of HeLa cells transfected with PCDH19FL-HA and subjected to a 20 min ionomycin treatment. Nuclei are counterstained with DAPI (blue). Relative nuclear fluorescence was quantified, mean ± SEM is displayed (N=15). Scale bar: 20 µm.

E. Western blot detection of full length and processed PCDH19 in cytoplasm/nucleus (C/N) and membrane (Mb) enriched fractions of MEF lysates (right). A western blot to verify the subcellular fractionation of MEF lysates into cytoplasm/nucleus and membrane enriched fractions is shown on the left.

Data information: Relative nuclear fluorescence was obtained by dividing nuclear fluorescence by the sum of nuclear and cytoplasmic fluorescence. N: individual cells. ***$p < 0.001$. Statistical analysis: two-tailed Mann-Whitney test.

Figure 3. PCDH19 ICD interacts with importins for nuclear transport.

A. Co-IPs of PCDH19FL (left) and PCDH19-ICD (right) with importin α1 (KPNA1).

B. HeLa cells transfected with PCDH19ICD-HA or PCDH19ICD-HA with a mutated NLS, and subjected to a 20 min ionomycin treatment. Representative confocal images of transfected cells immunostained for HA (left). Nuclei are counterstained with DAPI. Relative nuclear fluorescence was quantified, mean ± SEM is displayed (right, N=15). Scale bar: 20 µm.

C. Co-IP of PCDH19 and KPNA1 from P10 cortical lysates. Ips were performed with anti-PCDH19, anti-KPNA1 and IgG.

Data information: Relative nuclear fluorescence was obtained by dividing nuclear fluorescence by the sum of nuclear and cytoplasmic fluorescence. N: Individual cells. ****$p < 0.0001$. Statistical analysis: unpaired two-tailed Student's t-test.

Figure 4. Generation of a new mESC-line to investigate the nuclear function of PCDH19-ICD.

A. Experimental strategy.

B. Schematic of the targeting of the *Rosa26* locus to express PCDH19-ICD-HA.

C. WB of mESCs subclones, showing successful (1.2 and 1.18) and unsuccessful (1.3) targeting of the *Rosa26* locus. All clones express PCDH19, but only 1.2 and 1.18 show expression of PCDH19-ICD-HA.

D. DIV12 Neurons derived from 19ICD-OE mESCs stained for MAP2 (green) and HA (red). Nuclei are counterstained with DAPI (blue). Scale bar: 20 µm.

E. *Pcdh19* exon usage. Normalised counts plotted along genomic coordinates of *Pcdh19* in DIV8 mESC-derived neurons (blue: WT (N=3), red: 19ICD-HA (N=3)).

F. Principal component analysis on RNAseq results of DIV8 and DIV12 neuronal samples determined with DESeq2. Shapes indicate time points (DIV8, DIV12), colors indicate cell-

lines (WT, 19ICD-OE) and alpha scale indicates samples belonging to each of the three independent differentiations (1, 2, 3).

G. Correlation matrix showing hierarchical clustering of samples based on expression of all genes, determined with DESeq2. Blue scale represents distance between samples, with darker blue corresponding to smaller distances.

H. Venn diagram with total numbers of DEGs and comparison of common and unique up- and downregulated genes between WT (N=3) and 19ICD-OE (N=3) at DIV8 and DIV12, determined by RNAseq. The number of up- and downregulated genes is indicated by upward and downward arrows, respectively.

I. Expression levels of differentially expressed genes in mESC-derived neurons at DIV8 and DIV12, determined by RT-PCR (N=3).

Data information: cDNA quantity was obtained using a standard curve. For each of the 3 samples obtained from independent differentiations, 3 technical replicates were run, and their results were averaged. Data are presented as mean ± SEM. N: biological replicates (independent differentiations). Relevant P-values are indicated: *$p < 0.05$, **$p < 0.01$. Statistical analysis: two-tailed Mann-Whitney test (*Zic1* DIV8); unpaired two-tailed Student's t-test (rest).

Figure 5. Overexpression of PCDH19-ICD leads to transcriptional changes in neuronal differentiation-related genes in mESC-derived neurons.

A. Top 15 Biological Process GO-terms enriched among the differentially expressed genes at DIV8 as determined by gProfiler. Log(FDR) values are shown for each term. Common top 15 BP GO-terms between gProfiler, ShinyGO and Panther are highlighted in bold.

B. Log(FDR) values for the GO-terms "neurogenesis", "generation of neurons" and "neuron differentiation" at DIV12 across gProfiler, ShinyGO and Panther.

C. Top 15 Cellular Compartment GO-terms enriched among the differentially expressed genes at DIV8 as determined by gProfiler. Log(FDR) values are shown for each term. Common top 15 CC GO-terms between gProfiler, ShinyGO and Panther are highlighted in bold.

D. Venn diagram displaying the number of common and unique DEGs related to the three selected GO-terms at DIV8 and DIV12.

E. Diagram depicting the total number of DEGs for the GO-terms “neurogenesis”, “generation of neurons” and “neuron differentiation”, and how they relate to each other at DIV8 and DIV12.

F. List of significantly up- and downregulated genes between DIV8 WT and 19ICD-OE mESC-derived neurons related to the GO-term “neuronal differentiation” as determined by RNAseq. Genes are classified into transcription factors, membrane proteins and others, and their log2 fold change is depicted in green (upregulated) or pink (downregulated).

Figure 6. *In vivo* overexpression of PCDH19 ICD does not affect neuronal number, position or axonal trajectories of upper layer cortical neurons.

A. *In utero* electroporation to express PCDH19 ICD in upper layer cortical neurons. Strategy (top) and representative confocal images of electroporated brains immunostained for HA for the control (pCIG) and experimental (pCIG-19ICD-HA) conditions. Cortical layers are indicated with roman numerals. Scale bar: 200 µm.

B. Quantification (mean ± SEM) of the total number of electroporated neurons (top) and cortical thickness (bottom) for pCIG (N=7) and pCIG-19ICD-HA (N=11) brains.

C. Kernel density analysis of the distribution of electroporated cells for pCIG and pCIG-19ICD-HA electroporated brains.

D-E. Representative confocal images of the whole cortex of a pCIG (D) and a pCIG-19ICD-HA (E) electroporated brain showing axonal trajectories for the targeted neurons. Higher magnifications of the electroporated area (D’, E’), corpus callosum (D’’, E’’) and contralateral

hemisphere (D''', E''') are also shown. CTX: cortex, HIP: hippocampus, CC: corpus callosum. Scale bars: 500 μm for whole cortex, 200 μm for specific areas.

Data information: N: Biological replicate (electroporated brain). (B) Statistical analysis: unpaired two-tailed Student's t-test. No statistically significant differences identified. (C) Kernel density analysis was performed on pooled data for N=7 and N=11 electroporated brains for pCIG and pCIG-19ICD-HA, respectively. Statistical analysis: Kolmogorov-Smirnoff test between histogram distributions of neuronal positions using 50 μm bins. No statistically significant differences identified.

Figure 7. *In vivo* overexpression of PCDH19 ICD reduces spine density without affecting dendritic morphology.

A. Maximum intensity projections of confocal stacks showing individual upper layer neurons targeted with pCIG (left) or pCIG-19ICD-HA (right). Scale bar: 50 μm.

B. Examples of traced neurons electroporated with pCIG (top) or pCIG-19ICD-HA (bottom).

C. Quantification (mean ± SEM) of the width of the apical and basal dendritic arbors of pCIG (N=11) or pCIG-19ICD-HA (N=12) electroporated neurons, determined with the SNT plug in in Fiji.

D. Quantification (mean ± SEM) of the total dendritic length by dendrite order in pCIG (N=11) or pCIG-19ICD-HA (N=12) electroporated neurons, determined with the SNT plug in in Fiji.

E. Sholl analysis of pCIG (N=11) and pCIG-19ICD-HA (N=12) electroporated neurons, determined with the SNT plug in in Fiji.

F. Maximum intensity projections of confocal stacks showing apical and basal dendrites of pCIG and pCIG-19ICD-HA electroporated neurons at high magnification to visualize dendritic spines (63x objective). Fluorescent images have been inverted and are shown in greyscale to improve contrast. Scale bar: 10 μm.

G-I. Quantification (mean ± SEM) of total (G), apical (H) and basal (I) spine density in second order dendrites of pCIG (N=16) and pCIG-19ICD-HA (N=12) electroporated neurons.

Data information: (C, D) N: Individual neuron. No statistically significant differences identified. Statistical analysis: two-tailed Mann-Whitney test for apical and basal dendritic arbors (C); unpaired two-tailed Student's t-test for orders 1-4, two-tailed Mann-Whitney test for dendrite order 5. Analysis of orders 6 and 7 was not possible due to low numbers (D). (G-I): The average of all dendritic areas analyzed per neuron was used for the analysis of spine density. N: Individual neuron. Statistical analysis: two-tailed Mann-Whitney test for total and basal spine densities (G, I); unpaired two-tailed Student's t-test for apical spine density (H).

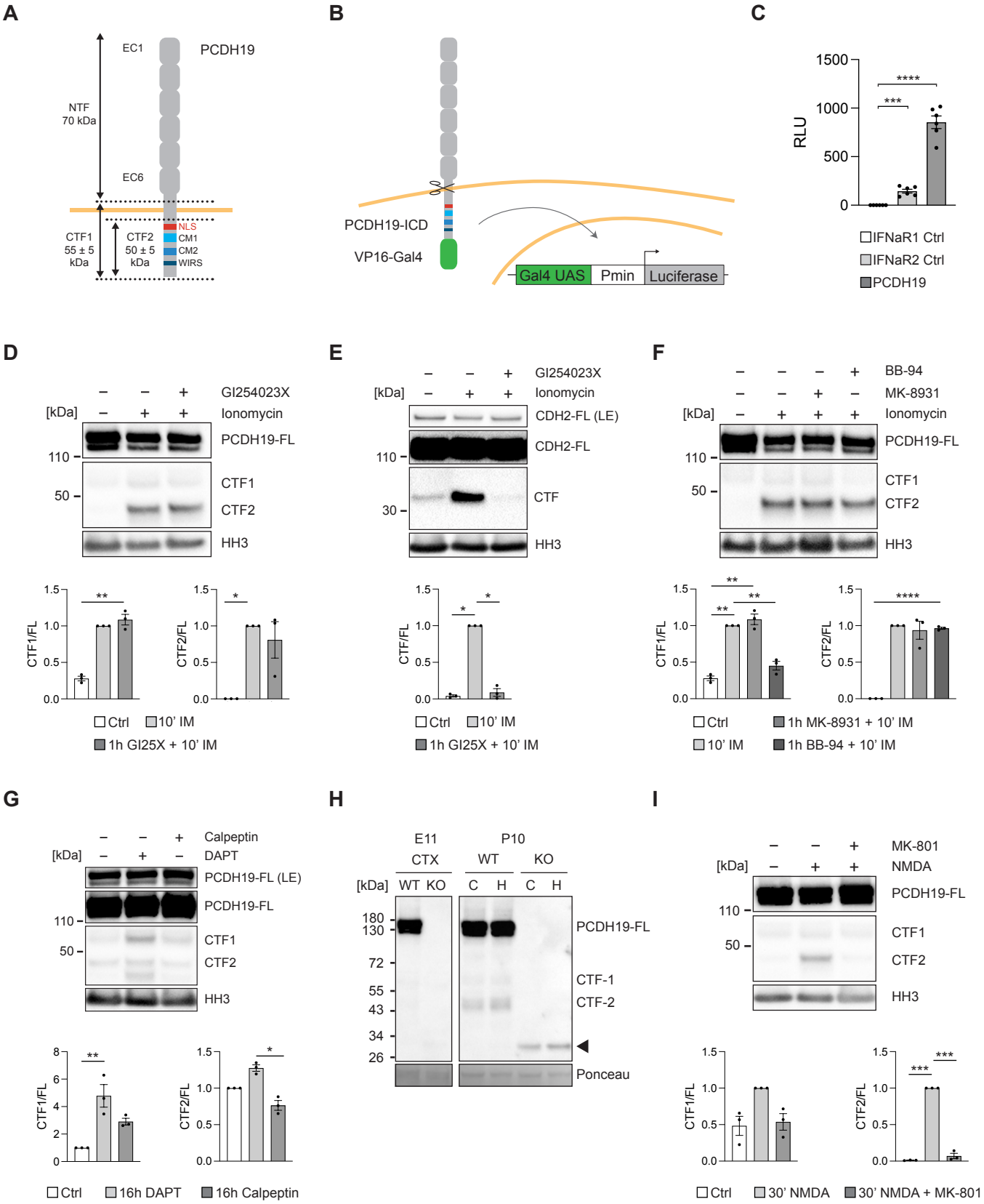
A
EC1
PCDH19
NTF
70 kDa
EC6
CTF1
55 ± 5
kDa
CTF2
50 ± 5
kDa
NLS
CM1
CM2
WIRS
B
PCDH19-ICD
VP16-Gal4
Gal4 UAS
Pmin
Luciferase
C
RLU
1500
1000
500
0
****
***
IFNaR1 Ctrl
IFNaR2 Ctrl
PCDH19
D
GI254023X
[kDa]
Ionomycin
PCDH19-FL
110
50
CTF1
CTF2
HH3
CTF1/FL
CTF2/FL
Ctrl
10' IM
1h GI25X + 10' IM
E
GI254023X
Ionomycin
CDH2-FL (LE)
CDH2-FL
CTF
30
CTF/FL
F
BB-94
MK-8931
Ionomycin
1h MK-8931 + 10' IM
1h BB-94 + 10' IM
G
Calpeptin
DAPT
PCDH19-FL (LE)
16h DAPT
16h Calpeptin
H
E11
P10
CTX
WT
KO
C
H
180
130
72
55
43
34
26
CTF-1
CTF-2
Ponceau
I
MK-801
NMDA
30' NMDA
30' NMDA + MK-801

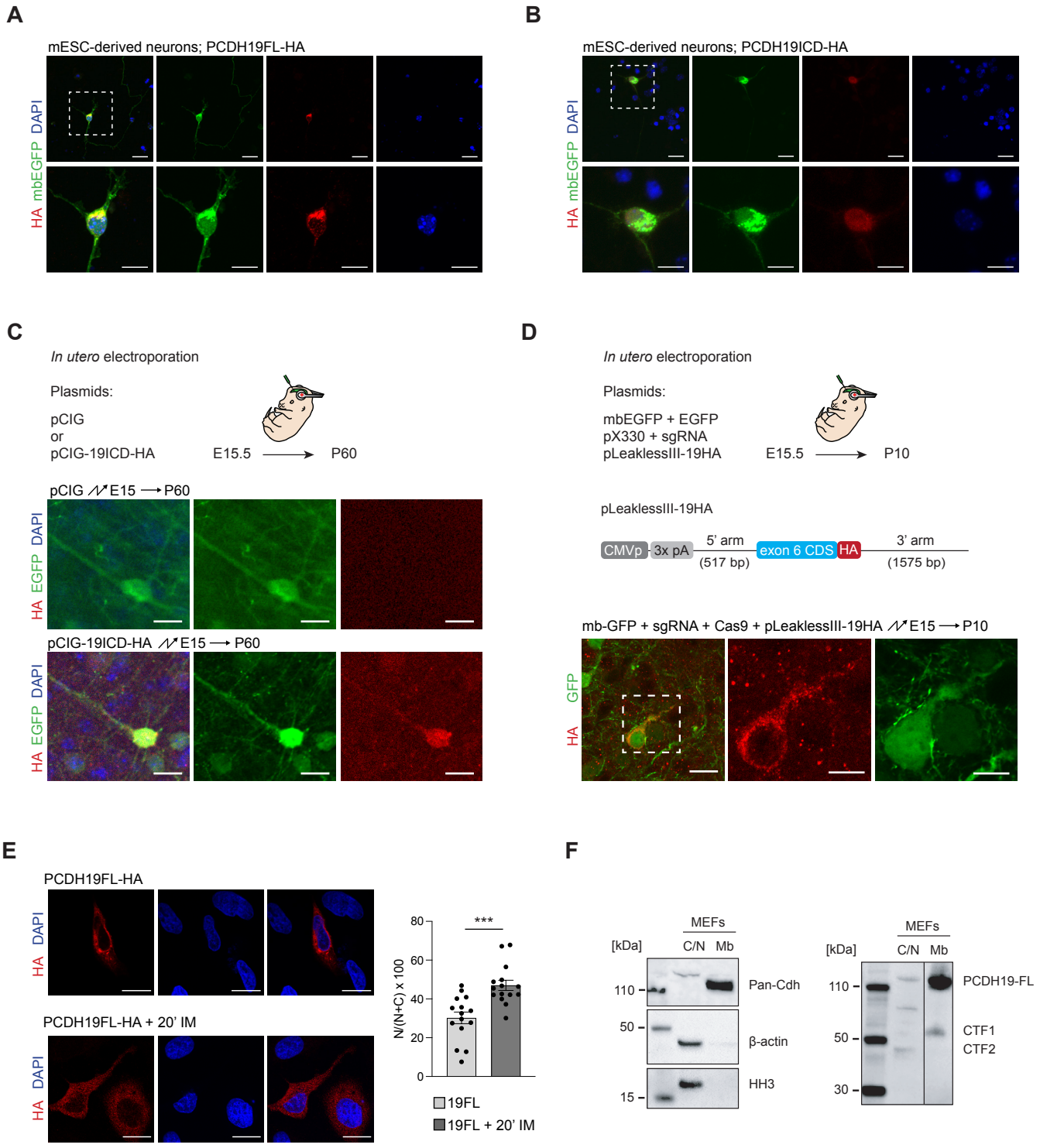
A
mESC-derived neurons; PCDH19FL-HA
DAPI
mbEGFP
HA
B
mESC-derived neurons; PCDH19ICD-HA
DAPI
mbEGFP
HA
C
In utero electroporation
Plasmids:
pCIG
or
pCIG-19ICD-HA
E15.5
P60
pCIG ⤳ E15 ⟶ P60
DAPI
EGFP
HA
pCIG-19ICD-HA ⤳ E15 ⟶ P60
DAPI
EGFP
HA
D
In utero electroporation
Plasmids:
mbEGFP + EGFP
pX330 + sgRNA
pLeaklessIII-19HA
E15.5
P10
pLeaklessIII-19HA
CMVp
3x pA
5' arm
(517 bp)
exon 6 CDS
HA
3' arm
(1575 bp)
mb-GFP + sgRNA + Cas9 + pLeaklessIII-19HA ⤳ E15 ⟶ P10
GFP
HA
E
PCDH19FL-HA
DAPI
HA
PCDH19FL-HA + 20' IM
DAPI
HA
***
N/(N+C) x 100
80
60
40
20
0
19FL
19FL + 20' IM
F
MEFs
[kDa]
C/N
Mb
110
50
15
Pan-Cdh
β-actin
HH3
MEFs
[kDa]
C/N
Mb
110
50
30
PCDH19-FL
CTF1
CTF2

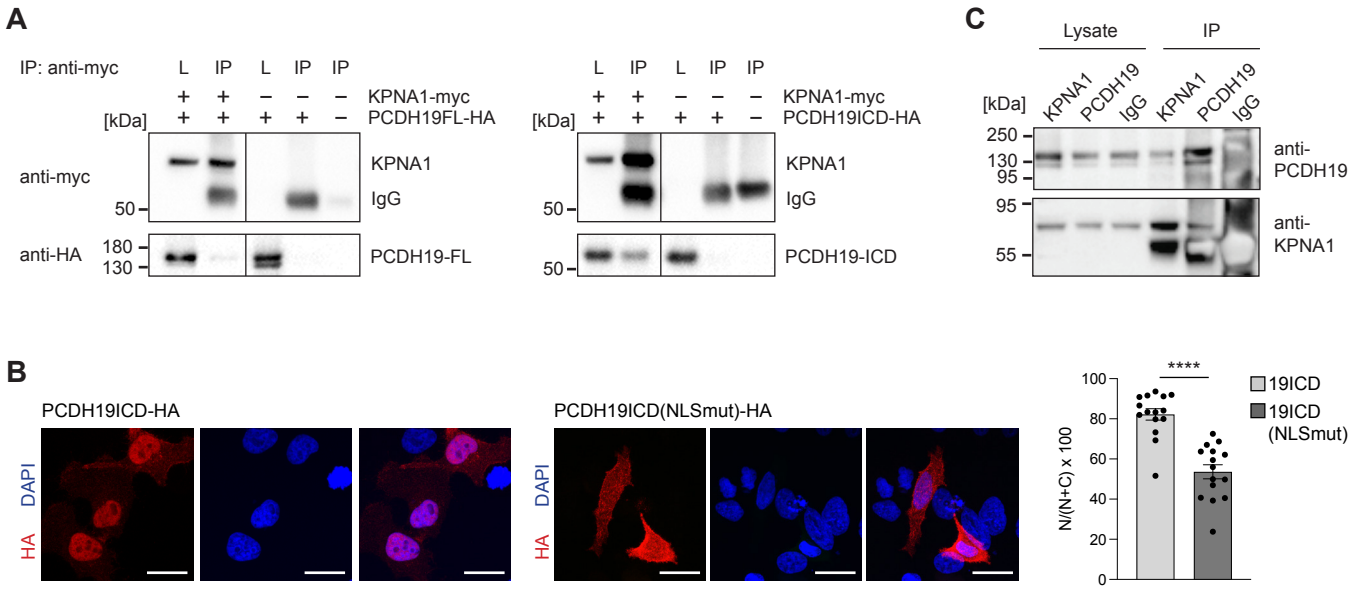
A
IP: anti-myc
L IP L IP IP
KPNA1-myc
PCDH19FL-HA
[kDa]
anti-myc
50
KPNA1
IgG
anti-HA
180
130
PCDH19-FL
L IP L IP IP
KPNA1-myc
PCDH19ICD-HA
[kDa]
50
KPNA1
IgG
50
PCDH19-ICD
C
Lysate
IP
[kDa]
KPNA1
PCDH19
IgG
KPNA1
PCDH19
IgG
250
130
95
anti-PCDH19
95
55
anti-KPNA1
B
PCDH19ICD-HA
DAPI
HA
PCDH19ICD(NLSmut)-HA
DAPI
HA
****
100
80
60
40
20
0
N/(N+C) x 100
19ICD
19ICD (NLSmut)

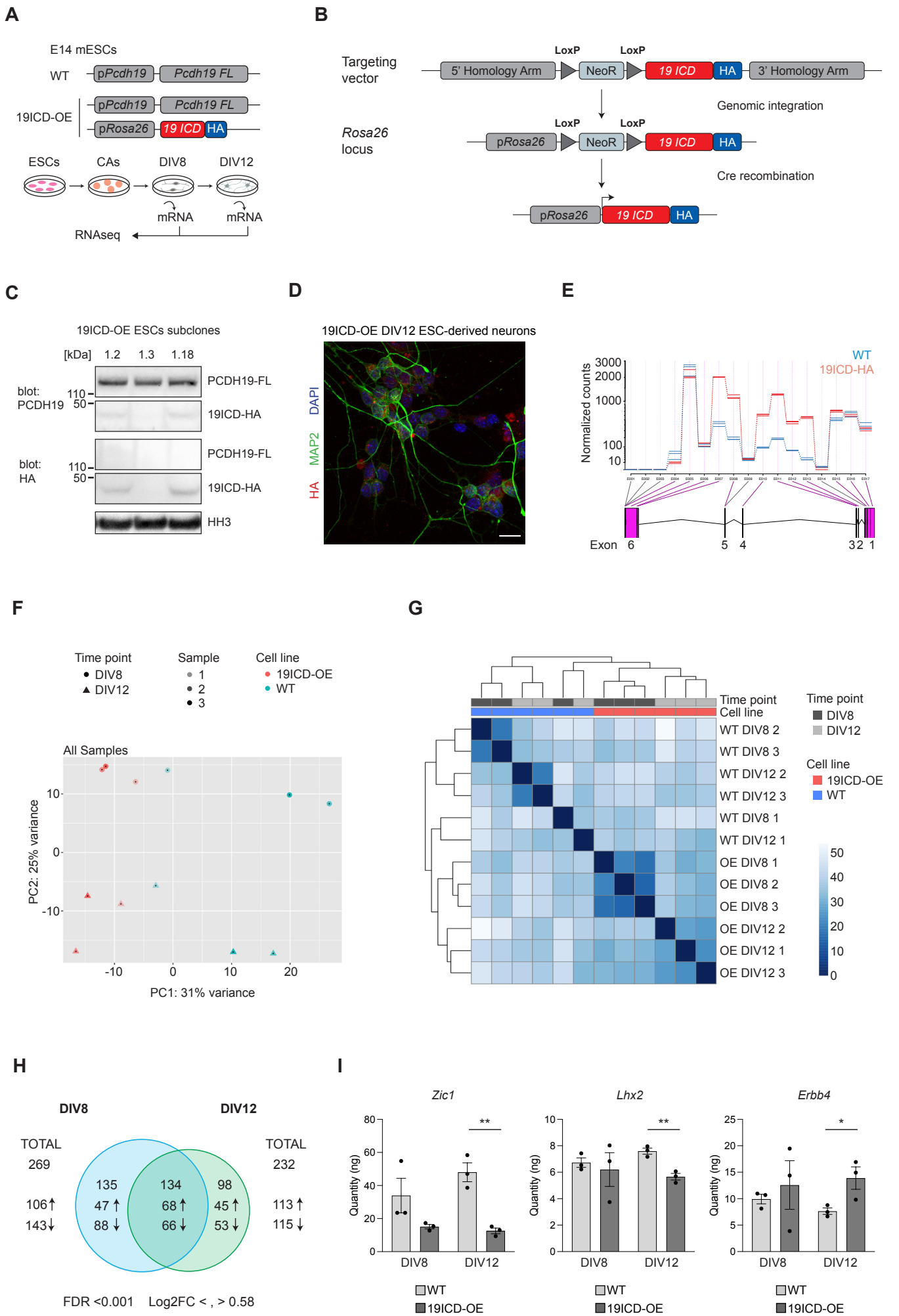
A
E14 mESCs
WT
pPcdh19
Pcdh19 FL
19ICD-OE
pPcdh19
Pcdh19 FL
pRosa26
19 ICD
HA
ESCs
CAs
DIV8
DIV12
mRNA
mRNA
RNAseq
B
Targeting vector
5' Homology Arm
LoxP
NeoR
LoxP
19 ICD
HA
3' Homology Arm
Genomic integration
Rosa26 locus
pRosa26
Cre recombination
C
19ICD-OE ESCs subclones
[kDa]
1.2
1.3
1.18
blot: PCDH19
110
50
PCDH19-FL
19ICD-HA
blot: HA
HH3
D
19ICD-OE DIV12 ESC-derived neurons
DAPI
MAP2
HA
E
WT
19ICD-HA
Normalized counts
3000
2000
1000
100
10
Exon
6
5
4
3
2
1
F
Time point
DIV8
DIV12
Sample
1
2
3
Cell line
19ICD-OE
WT
All Samples
PC2: 25% variance
PC1: 31% variance
G
Time point
Cell line
WT DIV8 2
WT DIV8 3
WT DIV12 2
WT DIV12 3
WT DIV8 1
WT DIV12 1
OE DIV8 1
OE DIV8 2
OE DIV8 3
OE DIV12 2
OE DIV12 1
OE DIV12 3
Time point
DIV8
DIV12
Cell line
19ICD-OE
WT
H
DIV8
DIV12
TOTAL
269
106↑
143↓
135
47↑
88↓
134
68↑
66↓
98
45↑
53↓
TOTAL
232
113↑
115↓
FDR <0.001
Log2FC < , > 0.58
I
Zic1
Lhx2
Erbb4
Quantity (ng)
DIV8
DIV12
WT
19ICD-OE

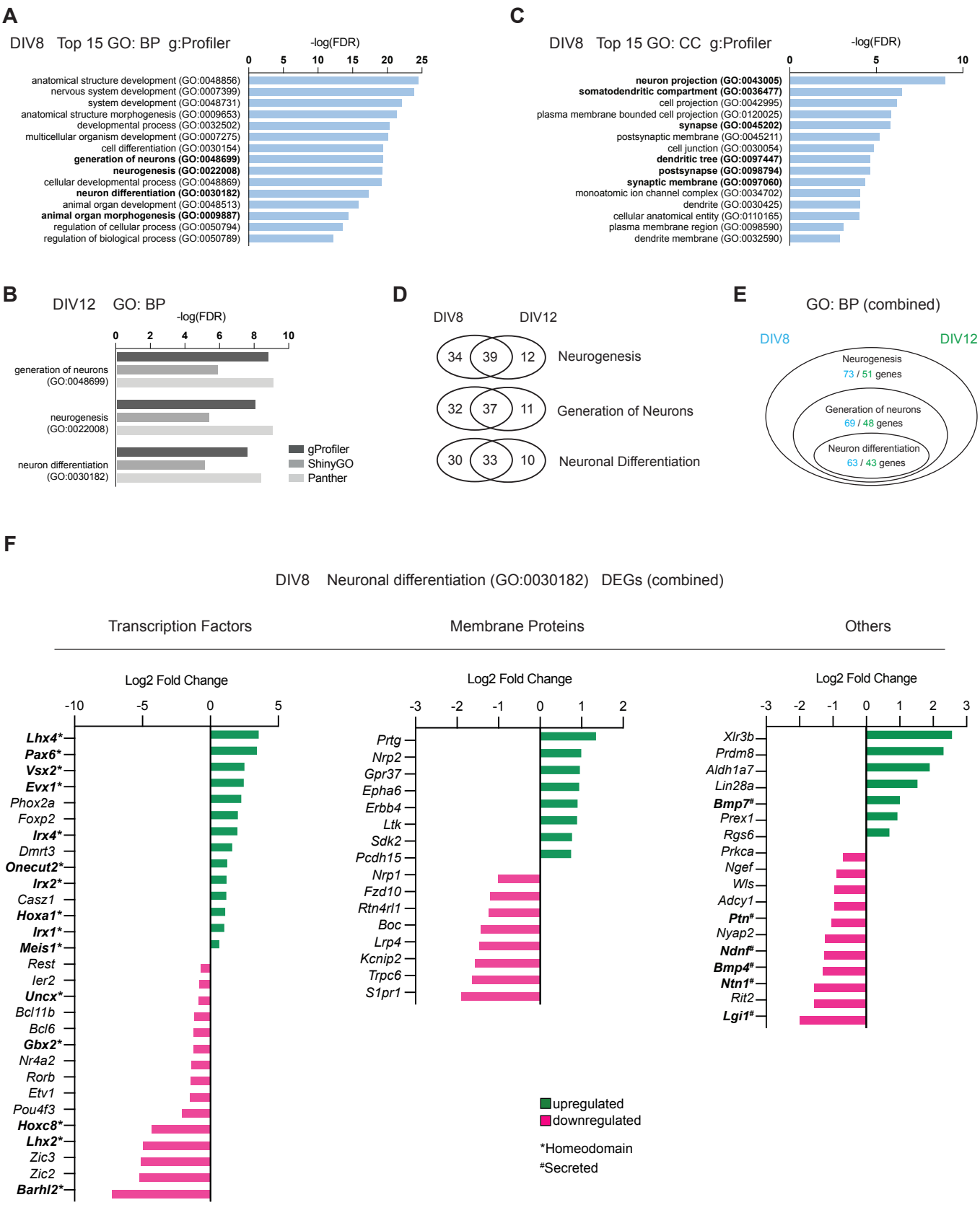
A
DIV8 Top 15 GO: BP g:Profiler
-log(FDR)
0 5 10 15 20 25
anatomical structure development (GO:0048856)
nervous system development (GO:0007399)
system development (GO:0048731)
anatomical structure morphogenesis (GO:0009653)
developmental process (GO:0032502)
multicellular organism development (GO:0007275)
cell differentiation (GO:0030154)
generation of neurons (GO:0048699)
neurogenesis (GO:0022008)
cellular developmental process (GO:0048869)
neuron differentiation (GO:0030182)
animal organ development (GO:0048513)
animal organ morphogenesis (GO:0009887)
regulation of cellular process (GO:0050794)
regulation of biological process (GO:0050789)
C
DIV8 Top 15 GO: CC g:Profiler
-log(FDR)
0 5 10
neuron projection (GO:0043005)
somatodendritic compartment (GO:0036477)
cell projection (GO:0042995)
plasma membrane bounded cell projection (GO:0120025)
synapse (GO:0045202)
postsynaptic membrane (GO:0045211)
cell junction (GO:0030054)
dendritic tree (GO:0097447)
postsynapse (GO:0098794)
synaptic membrane (GO:0097060)
monoatomic ion channel complex (GO:0034702)
dendrite (GO:0030425)
cellular anatomical entity (GO:0110165)
plasma membrane region (GO:0098590)
dendrite membrane (GO:0032590)
B
DIV12 GO: BP
-log(FDR)
0 2 4 6 8 10
generation of neurons (GO:0048699)
neurogenesis (GO:0022008)
neuron differentiation (GO:0030182)
gProfiler
ShinyGO
Panther
D
DIV8
DIV12
34 39 12 Neurogenesis
32 37 11 Generation of Neurons
30 33 10 Neuronal Differentiation
E
GO: BP (combined)
DIV8
DIV12
Neurogenesis
73 / 51 genes
Generation of neurons
69 / 48 genes
Neuron differentiation
63 / 43 genes
F
DIV8 Neuronal differentiation (GO:0030182) DEGs (combined)
Transcription Factors
Membrane Proteins
Others
Log2 Fold Change
-10 -5 0 5
Lhx4* Pax6* Vsx2* Evx1* Phox2a Foxp2 Irx4* Dmrt3 Onecut2* Irx2* Casz1 Hoxa1* Irx1* Meis1* Rest Ier2 Uncx* Bcl11b Bcl6 Gbx2* Nr4a2 Rorb Etv1 Pou4f3 Hoxc8* Lhx2* Zic3 Zic2 Barhl2*
Log2 Fold Change
-3 -2 -1 0 1 2
Prtg Nrp2 Gpr37 Epha6 Erbb4 Ltk Sdk2 Pcdh15 Nrp1 Fzd10 Rtn4rl1 Boc Lrp4 Kcnip2 Trpc6 S1pr1
Log2 Fold Change
-3 -2 -1 0 1 2 3
Xlr3b Prdm8 Aldh1a7 Lin28a Bmp7# Prex1 Rgs6 Prkca Ngef Wls Adcy1 Ptn# Nyap2 Ndnf# Bmp4# Ntn1# Rit2 Lgi1#
upregulated
downregulated
*Homeodomain
#Secreted

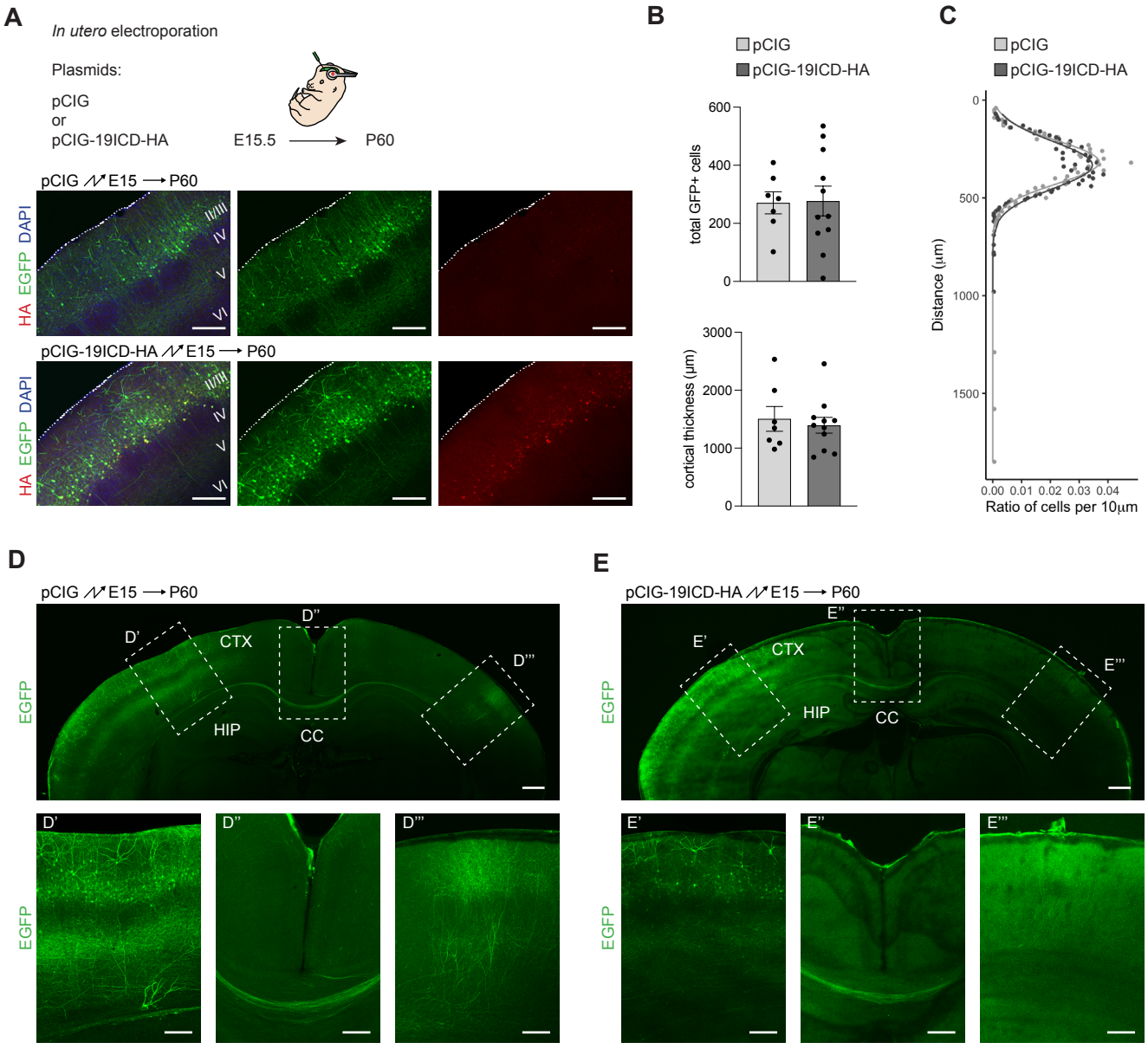
A
In utero electroporation
Plasmids:
pCIG
or
pCIG-19ICD-HA
E15.5
P60
pCIG ⤳ E15 ⟶ P60
pCIG-19ICD-HA ⤳ E15 ⟶ P60
DAPI
EGFP
HA
II/III
IV
V
VI
B
pCIG
pCIG-19ICD-HA
total GFP+ cells
cortical thickness (μm)
C
Distance (μm)
Ratio of cells per 10μm
D
CTX
HIP
CC
D'
D''
D'''
E
E'
E''
E'''

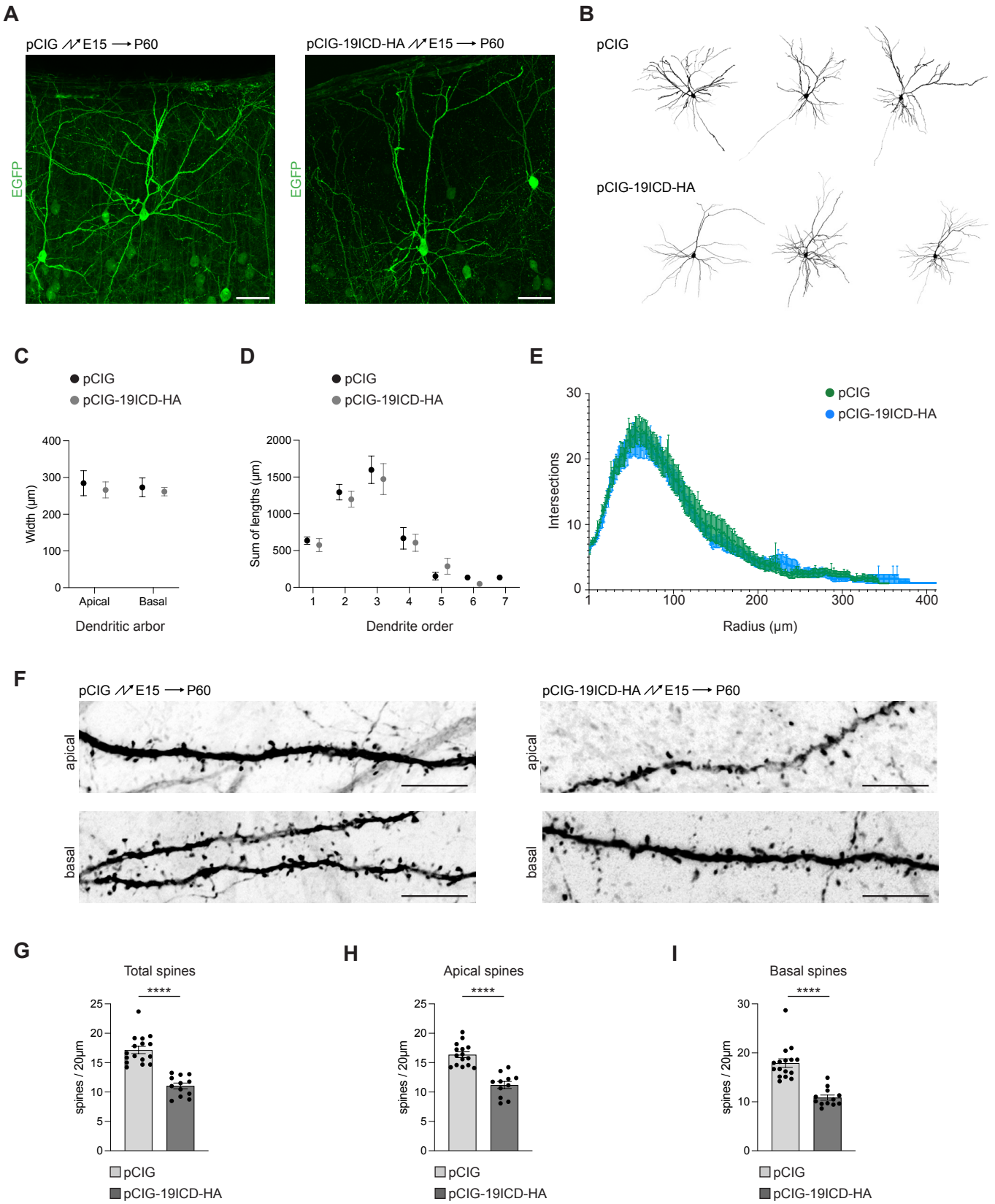
A
pCIG ⤴ E15 ⟶ P60
pCIG-19ICD-HA ⤴ E15 ⟶ P60
EGFP
EGFP
B
pCIG
pCIG-19ICD-HA
C
pCIG
pCIG-19ICD-HA
Width (µm)
400
300
200
100
0
Apical
Basal
Dendritic arbor
D
pCIG
pCIG-19ICD-HA
Sum of lengths (µm)
2000
1500
1000
500
0
1
2
3
4
5
6
7
Dendrite order
E
pCIG
pCIG-19ICD-HA
Intersections
30
20
10
0
1
100
200
300
400
Radius (µm)
F
pCIG ⤴ E15 ⟶ P60
pCIG-19ICD-HA ⤴ E15 ⟶ P60
apical
basal
apical
basal
G
Total spines
****
spines / 20µm
25
20
15
10
5
0
pCIG
pCIG-19ICD-HA
H
Apical spines
****
spines / 20µm
25
20
15
10
5
0
pCIG
pCIG-19ICD-HA
I
Basal spines
****
spines / 20µm
30
20
10
0
pCIG
pCIG-19ICD-HA